Spatial patterning of tissue volume deformation in schizophrenia reflects brain network architecture

Golia Shafiei[1], Ross D. Markello[1], Alexandra Talpalaru[2,3], Carolina Makowski[1], Matthias Kirschner[1], Gabriel A. Devenyi[2], Patric Hagmann[4], Neil R. Cashman[5], Martin Lepage[2], M. Mallar Chakravarty[2,3], Alain Dagher[1,†,∀], Bratislav Mišić[1,†,∀]

[1] *McConnell Brain Imaging Centre, Montréal Neurological Institute, McGill University, Montréal, Canada*
[2] *Cerebral Imaging Center, Douglas Mental Health University Institute, McGill University, Montréal, Canada*
[3] *Department of Biological and Biomedical Engineering, McGill University, Montréal, Canada*
[4] *Department of Radiology, Lausanne University Hospital (CHUV-UNIL), 1011 Lausanne, Switzerland*
[5] *Department of Medicine (Neurology), University of British Columbia, Vancouver, Canada*
†*Correspondence to: alain.dagher@mcgill.ca or bratislav.misic@mcgill.ca*
∀*These authors contributed equally to this work.*

(Dated: May 3, 2019)

Abstract

There is growing recognition that connectome architecture shapes cortical and subcortical grey matter atrophy across a spectrum of neurological and psychiatric diseases. Whether connectivity contributes to tissue volume loss or deformation in schizophrenia in the same manner remains unknown. Here we relate tissue volume loss in patients with schizophrenia to patterns of structural connectivity, functional connectivity, and gene expression. We find that regional deformation is correlated with the deformation of structurally- and functionally-connected neighbours. Distributed deformation patterns are circumscribed by specific functional systems (the salience network and default mode network), with an epicenter in the anterior cingulate cortex. Finally, areas most vulnerable to deformation are enriched for molecular pathways involved in synapse formation and cell-to-cell signaling, while areas that are protected are more likely to be enriched for pathways involved in immune and inflammatory responses. Altogether, the present study demonstrates that brain tissue volume loss in schizophrenia is conditioned by structural and functional connectivity, accounting for 30-40% of regional variance in deformation. The association between connectivity and deformation appears to have a molecular origin, reflecting an interplay between developmental/trans-neuronal and cellular immune mechanisms.

INTRODUCTION

The human brain is a complex network of anatomically connected and perpetually interacting neuronal populations. The connectivity of the network promotes inter-regional signaling, manifesting in patterns of synchrony and co-activation [6, 31]. The network also supports molecular transport, including molecules and organelles required for neurotransmission and metabolism [62]. Altogether, the architecture of this white matter "connectome" fundamentally shapes the development and function of the brain [30].

Despite many benefits for communication efficiency and resource sharing, networked systems are also vulnerable to damage [28]. Connections among elements allow pathological perturbations to spread between multiple nodes. Multiple neurodegenerative diseases, including Alzheimer's and Parkinson's diseases, are increasingly conceptualized as arising from trans-neuronal spread of pathogenic misfolded proteins [40, 87]. As a result, patterns of neurodegeneration resemble the underlying structural and functional architecture, and are often centered on one or more specific epicenters [72, 92, 95].

Widespread reductions in tissue volume are also observed in schizophrenia (hereafter referred to as *deformation*), but their origin remains unknown [44, 75, 78, 80, 82]. Patterns of cortical thinning in schizophrenia are highly organized and circumscribed by specific networks [58, 80], raising the possibility that connectome architecture shapes the pathological process. Anatomical connections may potentially allow pathogens, such as misfolded proteins or inflammatory markers, to propagate between regions [28]. Additionally, transport of trophic factors between regions may be disrupted if white matter projections are compromised. Both mechanisms would lead to cortical and subcortical deformation patterns that reflect the white matter architecture (i.e., white matter connectivity patterns). Several recent studies have found evidence consistent with this idea. For example, cortical thinning and infracortical white matter breakdown (as measured by fractional anisotropy) appear to be concomitant in patients with schizophrenia [20] and in patients with de novo psychotic illness [48]. In addition, cortical thinning is more pronounced among regions with stronger grey matter covariance [86]. Altogether, there is considerable - though circumstantial - evidence that connectivity influences deformation patterns.

Here we test the hypothesis that distributed deformation patterns in schizophrenia are conditioned by connectome architecture. We first estimate cortical and subcortical grey matter deformation in a sample of $N = 133$ patients with schizophrenia. We also derive structural and functional networks from independent samples of healthy participants. We then investigate whether deformation

patterns are more likely to be concentrated within subnetworks, and whether regions that experience greater deformation are also more likely to be connected with each other. Finally, we explore how local mRNA transcription patterns mediate this relationship. We demonstrate that grey matter loss is systematically related to connectome architecture and that this relationship has a molecular (gene expression) signature.

RESULTS

The results are organized as follows. We first establish disease-related patterns of grey matter deformation using mass-univariate contrasts, which isolate patterns of deformation that differentiate patients and controls. We then investigate whether the spatial patterning of schizophrenia-related deformation can be explained by structural connectivity, functional connectivity, and gene transcription. We demonstrate that the network dependence of deformation is not trivially confounded by spatial proximity or network resolution. Data sources include (see *Materials and Methods* for detailed procedures):

- *Grey matter deformation.* Grey matter deformation was estimated in a sample of $N = 133$ individuals with chronic schizophrenia and $N = 113$ controls (source: Northwestern University Schizophrenia Data and Software Tool; NUSDAST [42]). Deformation-based morphometry (DBM) was used to estimate cortical and subcortical grey matter deformation from T1-weighted MR images [5, 14, 17, 45, 76, 95].

- *Structural connectivity.* Structural and functional connectivity were derived from $N = 70$ healthy control participants (source: Lausanne University Hospital). Structural connectivity was reconstructed using diffusion spectrum imaging and deterministic streamline tractography. A consistency- and length-based procedure was then used to assemble a group-representative structural connectivity matrix [9, 53, 54].

- *Functional connectivity.* Functional connectivity was estimated in the same individuals using resting-state functional MRI (rs-fMRI). A functional connectivity matrix was constructed using pairwise Pearson correlations among regional time courses. A group-average functional connectivity matrix was then estimated as the mean connectivity of pair-wise connections across individuals.

- *Gene expression.* Regional mRNA transcription profiles were derived using *in situ* hybridization in six individuals post-mortem (source: Allen Institute Human Brain Atlas) [37].

System-specific deformation

Schizophrenia-related deformation was first defined by contrasting the deformation maps of schizophrenia patients and healthy controls, using a mass-univariate analysis (i.e., two-tailed two-sample t-test) of voxel-wise differences between DBM values of the two groups. The deformation pattern shown in Fig. 1a appears to mainly target brain regions associated with the default-mode and salience networks. To statistically assess if this is the case, we used a spatial permutation procedure (Fig. 1b). Voxels were first parcellated according to the multi-resolution Lausanne anatomical atlas [13]. The atlas features five progressively finer parcellations, from 83 to 1015 regions or nodes (i.e., 83, 129, 234, 463, 1015). Separately, voxels were assigned to one of the 264 brain regions according to the atlas reported by Power and colleagues [64]. Nodes defined by the Lausanne and Power atlases were stratified according to their membership in functional MRI resting-state networks previously reported by Yeo and colleagues [93] and by Power and colleagues [64], respectively. We first calculated the mean deformation value (i.e., mean z-statistic) within each network. We then randomly permuted network assignments of each node while respecting hemisphere assignments, and re-calculated the mean deformation for each network (Fig. 1b). The procedure was repeated 10,000 times and used to construct a distribution of network deformation means under the null hypothesis that regional deformation patterns are independent of affiliation with these large-scale systems.

Fig. 1c shows the mean deformation values (expressed as z-scores relative to the null distribution) for each network. Consistent with the voxel-wise anatomical pattern, the default mode (DM) and ventral attention (VA) networks among Yeo networks and the default mode (DM) and salience (SAL) networks among the Power networks are associated with the greatest deformation. Fig. 1c further confirms this notion: relative to the label-permuting null model, the default mode network (for both Yeo and Power networks) as well as ventral attention (for Yeo) and salience (for Power) networks have the greatest z-score, suggesting that the observed deformation patterns are significantly greater in these networks. Note that the ventral attention network defined by Yeo and colleagues [93] highly overlaps with the salience network defined by Power and colleagues [64].

Structural and functional connectivity shape deformation

The fact that tissue volume loss is circumscribed to specific intrinsic networks suggests that deformation may be constrained by network architecture. We therefore directly test the possibility that the distribution of deformation patterns in schizophrenia is shaped by structural and functional connectivity. If this is the case, nodes strongly connected with high-deformation neighbours

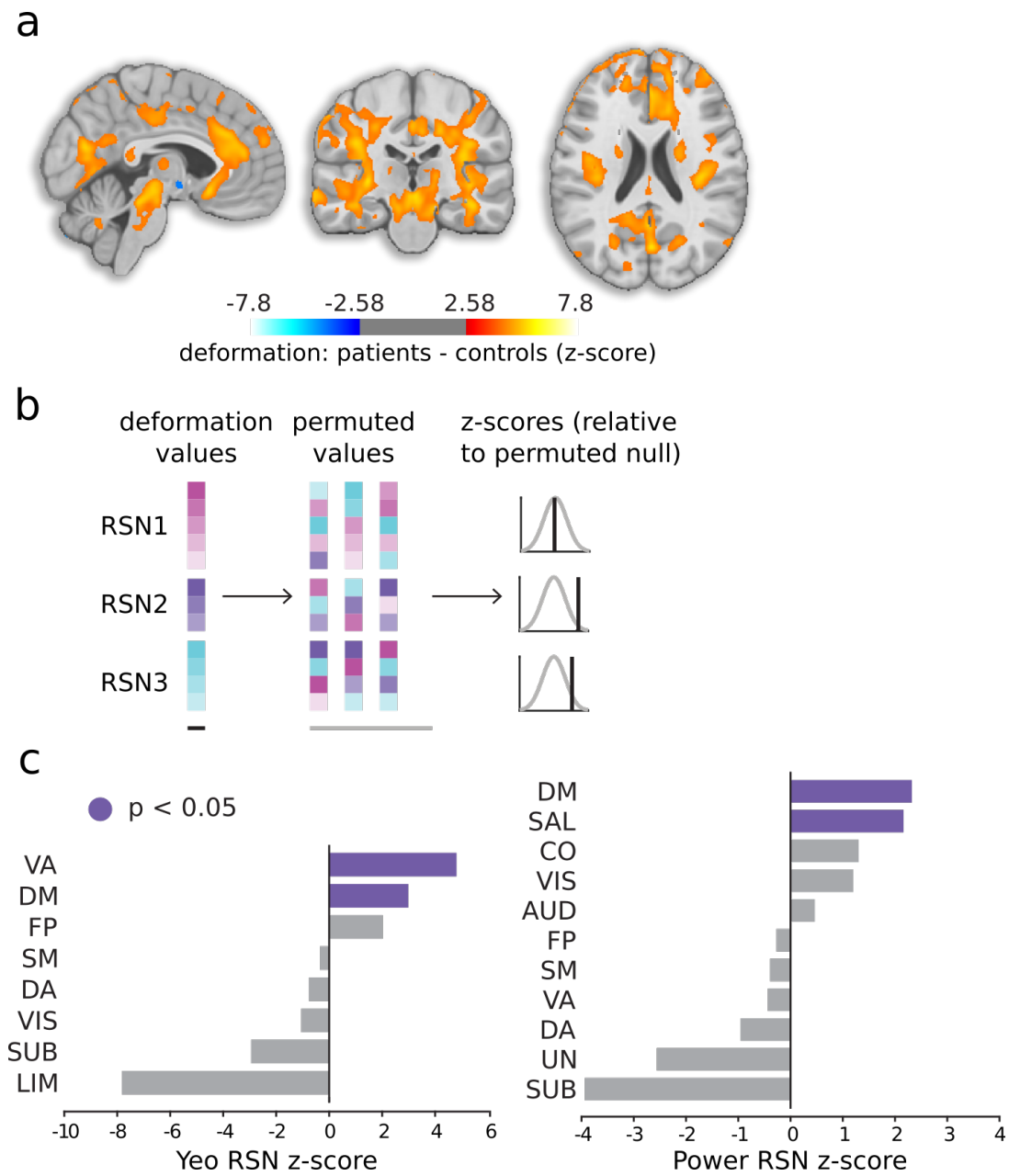

Figure 1. **Deformation in schizophrenia patients compared to healthy controls |** (a) Deformation-based morphometry maps of schizophrenia patients and controls were contrasted using two-sample t-tests. The t-statistics are converted to z-scores and displayed on an MNI template (MNI152_symm_2009a; ($x = -4$, $y = -23$, $z = 22$)). Greater z-scores correspond to greater deformation in schizophrenia patients relative to healthy controls. The maps are corrected for multiple comparisons by controlling the false discovery rate at 5% [7]. (b) The deformation pattern is stratified into resting-state networks (RSNs) defined by Yeo and colleagues [93] and Power and colleagues [64]. The mean deformation score is calculated for each network. Network labels are then permuted and network-specific means are re-calculated. The procedure is repeated 10,000 times to generate a null distribution of network-specific deformation. (c) Mean deformation for each RSN, expressed as a z-score relative to the null distribution generated by the label-permuting procedure. Yeo networks: DM = default mode, DA = dorsal attention, VIS = visual, SM = somatomotor, LIM = limbic, VA = ventral attention, FP = fronto-parietal, SUB = subcortical areas (defined based on the anatomical Desilan-Killiany parcellation [19]). Power networks: DM = default mode, SAL = salience, CO = cingulo-opercular task control, VIS = visual, AUD = auditory, FP = fronto-parietal task control, SM = sensory/somatomotor (hand and mouth combined), VA = ventral attention, DA = dorsal attention, UN = uncertain and memory retrieval combined, SUB = subcortical areas.

should display greater deformation, while nodes connected mainly with low-deformation neighbours should display less deformation (Fig. 2a).

To test this hypothesis, we investigate whether the deformation of a given brain region is correlated with the deformation of its connected neighbours. We derive structural and functional connectivity from an independent sample of $N = 70$ participants. Structural connectivity was estimated using diffusion weighted imaging and deterministic streamline tractography, while functional connectivity was estimated using resting-state functional MRI (rs-fMRI) (see *Materials and Methods* for more details). Structural and functional data were then parcellated into five progressively finer parcellations (from 83 to 1015 nodes) [13]. Parcellated data was used to construct group-representative structural and functional connectivity networks [9, 54].

For each network node, we correlate the local schizophrenia-related deformation value (z-score) with the normalized sum of its structural or functional neighbours' deformation values (Fig. 2a). In the case of structural connectivity, the neighbours are defined as the regions connected to each node with an underlying structural connection from diffusion spectrum imaging. In the case of functional connectivity, the neighbours' deformation values are weighted by the temporal zero-lag Pearson correlation coefficients. The sum is then normalized by the number of connections of the node with its neighbours, effectively correcting for node degree. For both structural and functional connectivity, the deformation of a node is significantly correlated with the deformation of its connected neighbours (resolution 3; $r = 0.52, P = 1.53 \times 10^{-17}$ and $r = 0.55, P = 3.92 \times 10^{-20}$ respectively; Fig. 2b,c). The results are consistent when we simultaneously include both structurally- and functionally-defined neighbours' deformation estimates as predictors in a multiple regression model (resolution 3; adjusted-$r = 0.57, P = 7.23 \times 10^{-21}$; Table S1).

We next seek to assess the extent to which these associations depend on network topology. To address this question, we constructed two null models: (1) a null structural model by randomly rewiring pairs of edges in the structural network [49]; (2) a null functional model by randomly reassigning rs-fMRI time series to each node. Fig. 2d shows the correlations between nodes' and neighbours' deformation values across the five resolutions using empirical structural and functional networks (black), as well as the corresponding correlations using the null structural and functional networks (100 repetitions). In both instances, the overall correspondence between node and neighbour deformation is greater in the empirical network than the null network ($P < 0.01$).

Finally, we test whether functional connectivity on its own - without reference to the underlying structural patterns - could be used to predict deformation among nodes. To address this question, we first computed the correlations between node and neighbour deformation (weighed by functional connectivity) for structurally connected neighbours (Fig. 2e; black). We also computed associations between nodes and non-structurally connected neighbours (Fig. 2e; grey). Fig. 2e shows that the associations remain only when considering structurally connected neighbours. In other words, functional connectivity between nodes is associated with their mutual deformation, but only if there exists an underlying white-matter connection. Although we identify strong influence of directly-connected neighbours, there is little evidence that neighbours further than one hop away make a reliable contribution to local deformation according to our analysis.

Identifying the disease epicenter

Given that schizophrenia-related deformation depends on structural and functional connectivity, we next ask which brain regions might be the putative epicenters of the disease, analogous to the source of an epidemic. We hypothesized that a high-deformation node could potentially be an epicenter if its neighbours also experience high deformation (Fig. 2f). Nodes were ranked based on their deformation values and their neighbours' deformation values in ascending order in two separate lists; we then identified nodes that were highly ranked in both lists. Fig. 2g shows that areas with highest mean rankings across both lists are primarily located in the bilateral cingulate cortices, consistent with previous literature [18]. Left paracentral lobule and left transverse temporal gyrus are the other highly ranked regions after the cingulate cortices. It should be noted that we included subcortical areas (not shown in Fig. 2g) in the epicenter analysis, but they were not among the nodes with high mean rankings (ranked around or below the 50th percentile). To ensure that the effect is not driven by the number of connections (i.e. biased towards high-degree nodes), we normalized the deformation values of neighbours' of a given node by its degree.

Interestingly, the highly ranked areas have been reported to be enriched for von Economo neurons [1, 12, 15]. Von Economo neurons are large bipolar neurons that are primarily distributed in anterior cingulate and frontoinsular cortices in human brain and are shown to be involved in schizophrenia and other psychiatric disorders [1, 12, 15]. The fact that the potential epicenter seems to be localized to these regions opens the possibility that deformation may be related to cytoarchitectonic characteristics. Therefore, we investigated tissue volume deformation relative to the cytoarchitectonic classification of human cortex according to the classic von Economo atlas [71, 84, 85]. Fig. 3a shows the mean deformation values for each von Economo cytoarchitectonic class, expressed as a z-score relative to a null distribution of class means generated by the label-permuting procedure explained above. We used an extended version of the von Economo cytoarchitectonic partition with 7 classes (Fig. 3b) that was previously defined by Vértes and colleagues [83]. Consistent with the voxel-wise anatomical

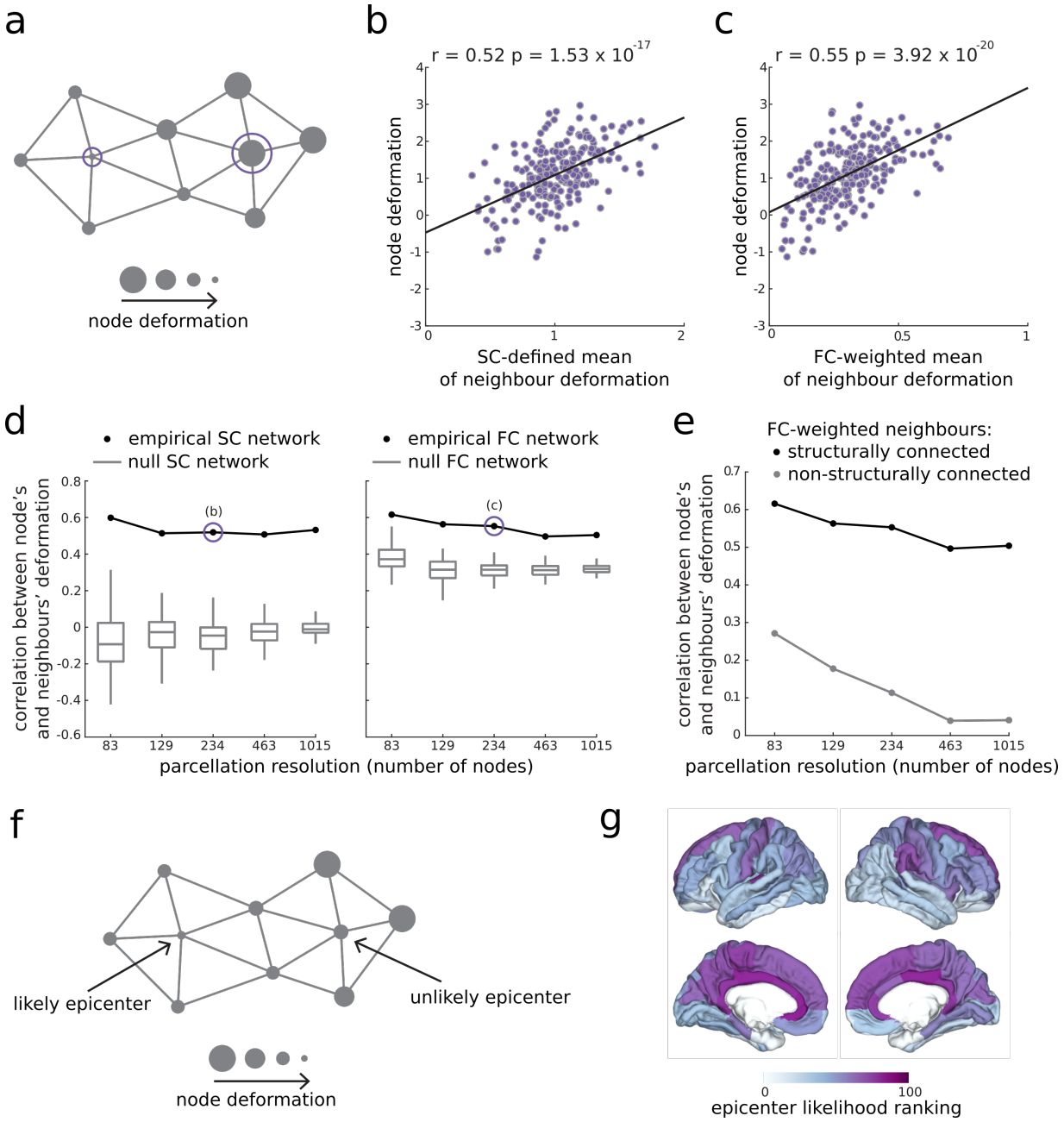

Figure 2. **Network-dependent deformation** | (a) Schematic of deformation of a node and its neighbours. If regional deformation depends on network connectivity, nodes connected to highly deformed neighbours will be more likely to be deformed themselves, while nodes connected to healthy neighbours will be less likely to be deformed. (b) The deformation of a node is correlated with the deformation of its neighbours defined by structural connectivity, estimated from an independently-collected diffusion-weighted MRI dataset. (c) The deformation of a node is correlated with the deformation of its neighbours weighted by functional connectivity, estimated from an independently-collected resting state functional MRI dataset. Both results are shown for the third resolution only (234 nodes). See Fig. S1 for results in all 5 resolutions, with and without the effect of distance regressed out from the data. (d) A null structural model was constructed by randomly rewiring pairs of edges in the structural network. A null functional model was also constructed by randomly reassigning resting-state functional MRI time series to each node. The correlations between nodes' and neighbours' deformation values are depicted across the five resolutions using empirical structural and functional networks (black), as well as the corresponding correlations using the null structural and functional networks (100 repetitions). (e) The correlations between node and neighbour deformation (weighed by functional connectivity) for structurally connected neighbours (black) were compared to the ones for non-structurally connected neighbours (grey). The associations remain only when considering structurally connected neighbours. (f) We hypothesized that a high-deformation node could potentially be an epicenter if its neighbours also experience high deformation. (g) The nodes were ranked based on their deformation values and their neighbours' deformation values in ascending order. The highly ranked nodes in both lists are primarily located in the bilateral cingulate cortices. Left paracentral lobule and left transverse temporal gyrus are the other highly ranked regions after the cingulate cortices. Note that subcortical areas (not shown in the figure) were also included in the analysis, but they were not among the highly ranked nodes (ranked below the 50th percentile).

deformation pattern (Fig. 1a) and with the results of epicenter analysis (Fig. 2), the insular (IC) and limbic (LB) regions among the von Economo cytoarchitectonic classes are associated with significantly greater deformation (Fig. 3).

Gene enrichment and deformation

Finally, we ask whether the observed deformation patterns depend on patterns of gene expression. Given the neurodevelopmental and genetic origins of schizophrenia, it is likely that the observed link between tissue volume loss and anatomical connectivity has a molecular origin. To test this hypothesis, we assess the relationship between grey matter deformation and mRNA transcription derived from the Allen Human Brain Atlas (AHBA) [37] (See *Materials and Methods*).

Using partial least squares (PLS) analysis, we first identified a linear combination of genes associated with regional variance in grey matter deformation [52, 83, 89]. The analysis was repeated for the first 3 parcellation resolutions (i.e., 83, 129, and 234 nodes), given the higher reliability of the microarray expression data for the medium and lower resolutions compared to finer ones (See *Materials and Methods*). PLS analysis identified a significant relationship between local brain deformation and gene expression for all 3 parcellations (permuted P-value = 0.002, 0.002, and 0.003 for 83, 129, and 234 nodes, respectively). The resulting loadings were split into positive and negative values (e.g., resolution 3: 9,300 and 11,297 genes, respectively) to create two ranked lists of genes, corresponding to positive and negative associations between gene expression and deformation, respectively. The ranked lists were submitted to an online gene ontology (GO) functional enrichment analysis tool, GOrilla [22, 23], and the resulting GO terms were summarized using REViGO [77] (See *Materials and Methods*). The results were consistent among all 3 parcellations, such that the PLS-derived loadings were highly correlated between the resolutions ($r \approx 0.9$ and $P \approx 0$) resulting in highly overlapped sets of genes and GO terms.

The summarized GO terms associated with greater and lower deformation are shown in Tables 1 and 2, respectively, for the third resolution parcellation (234 nodes). Consistent with the notion that deformation is related to connectivity, positive-deformation gene sets showed enrichment for processes associated with network development and function, including nervous system development (*regulation of neuron projection development*, *regulation of cell projection organization*) and cell communication and signaling (*trans-synaptic signaling*, *MAPK cascade*, *regulation of secretion*, *regulation of transport*). In other words, regional deformation patterns might be associated with altered gene expression of gens responsible for normal nervous system development. Interestingly, negative-deformation gene sets were enriched for processes associated with immune function, including *immune response*, *inflammatory response*, *detection of external biotic stimulus*, *leukocyte activation* and *macrophage activation*. Full GO tables for both sets are included in the *Supplementary Information* (Tables S2 and S3).

Control analyses: spatial proximity, parcellation resolution and medication

Given that deformation morphometry entails spatial smoothing, it is possible that the present results could be trivially driven by the parcellation used or by simple spatial proximity between nodes. We first repeated the analysis across five parcellation resolutions (ranging from 83 to 1015 cortical and subcortical nodes) and found that the results are generally consistent (Fig. S1, top). In other words, the relationship between connectivity and atrophy is robust to how network nodes are defined.

Likewise, it is possible that local deformation correlates with the deformation of connected neighbours because spatially proximal nodes trivially exhibit greater co-deformation and greater connectivity. To rule out this possibility, we regressed out the Euclidean distance between each node and its neighbours prior to calculating the weighted sum of neighbour deformation. As before, the deformation of a node was correlated with the deformation of its structural and functional neighbours, across resolutions (Fig. S1, bottom). We also repeated both analyses using a multiple regression model where deformation estimates of both structural and functional neighbours of a node were included as predictors, resulting in the same or slightly improved relationship between deformation of a node and its neighbours across resolutions (Table S1).

Finally, we sought to investigate the effects of chlorpromazine equivalent antipsychotic medication dose on spatial patterning of atrophy [82]. To address this question we removed all participants for whom current antipsychotic medication dose was not available. For the remaining 87 participants (64 second-generation, 10 first-generation, 7 both, 6 non-medicated), we computed the chlorpromazine equivalent dosage [61, 91]. We then repeated the analyses described above, controlling for medication dose in addition to age. We find that the medication-corrected DBM z-maps are highly correlated with the non-medication corrected maps ($r = 0.86$, $P \approx 0$ at resolution 3; Fig. S2). Moreover, we find that the relationship between neighbour connectivity and atrophy is still present and remains independent of spatial proximity and choice of parcellation (Fig. S3).

DISCUSSION

The present study demonstrates that brain tissue volume loss in schizophrenia is conditioned by structural and functional connectivity, accounting for 30-40% of regional variance in deformation. The association between connectivity and deformation appears to reflect an interplay between developmental/trans-neuronal and cellular

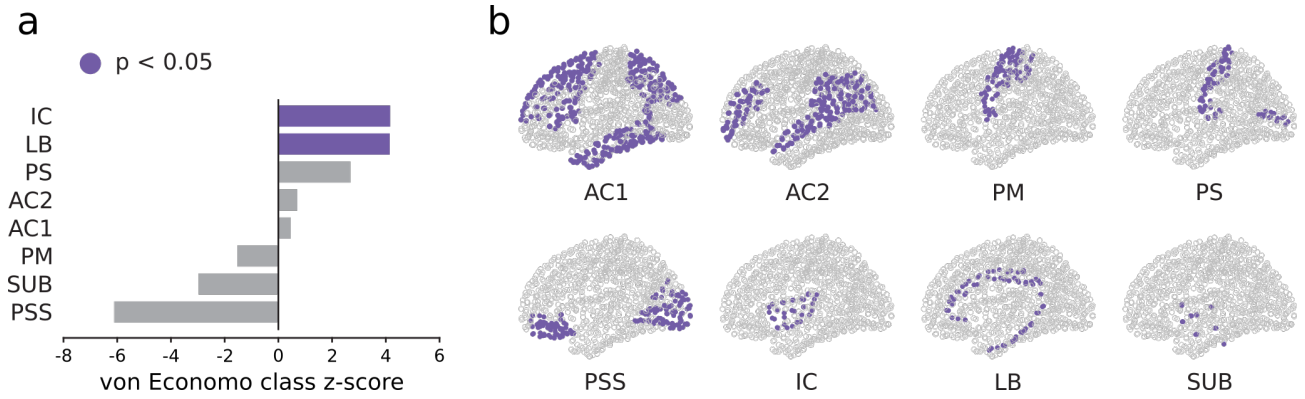

Figure 3. **von Economo cytoarchitectonic classification** | (a) Mean deformation for each von Economo cytoarchitectonic class [83, 84], expressed as a z-score relative to the null distribution generated by the label-permuting procedure. (b) Brain regions are visualized according to their assignment to each von Economo cytoarchitectonic class. AC1 = association cortex, AC2 = association cortex, PM = primary motor cortex, PS = primary sensory cortex, PSS = primary/secondary sensory, IC = insular cortex, LB = limbic regions. SUB = subcortical areas (according to the anatomical Desilan-Killiany parcellation [19]).

immune mechanisms.

Network patterning of deformation

The principal finding in the present investigation is that the deformation of an area is associated with the deformation of areas it is connected with. Interestingly, several recent studies found complementary results. Wannan and colleagues found that cortical thinning in schizophrenia was more likely among areas with greater anatomical covariance [86]. Di Biase and colleagues found that cortical thinning and reduction in local white matter anisotropy are anticorrelated in patients with schizophrenia [20]. Finally, Palaniyappan and colleagues found that patterns of cortical thinning are highly structured and systematically deviate from healthy anatomical covariance patterns [58]. Altogether, these results show that deformation patterns reflect network architecture, raising the possibility that connections drive pathology.

The structurally-guided deformation appears to accumulate in specific systems: the functionally-defined salience and default mode networks, and the cytoarchitectonically-defined insular and limbic classes. Moreover, given the structural connectome and the observed deformation pattern, we find that the likeliest epicenters are located in the cingulate cortices. These loci—situated at the intersection of the salience and default networks—are implicated in schizophrenia, including changes in tissue volume [27], structural connectivity [74, 94], activation [59, 60], and functional connectivity [11, 73, 90]. Interestingly, the same areas are frequently found to be affected in a wide range of mental illnesses, including schizophrenia, bipolar disorder, depression, addiction, obsessive-compulsive disorder and anxiety [34]. These regions may be particularly vulnerable because they are rich in von Economo neurons (VENs), which have also been associated with multiple psychiatric disorders including schizophrenia [1, 12, 15]. In addition to the bilateral cingulate cortices, we identify other brain regions that can potentially be the next likeliest epicenters. Left transverse temporal gyrus is one of such areas that has previously been related to schizophrenia, expressing cortical thinning and grey matter volume reduction [41, 56].

Despite the strong influence of directly-connected neighbours, we find little evidence that neighbours further than one hop away make a reliable contribution to local deformation. In other words, network connectivity plays an important role in shaping deformation but the influence is expressed mainly via direct connections and is more difficult to detect at longer path lengths. This result suggests the presence of additional, perhaps local, factors that shape deformation beyond the global connection patterns. As we describe below, one such factor appears to be gene transcription.

Genetic contributions to deformation

Although deformation is associated with structural and functional connectivity, we also find evidence of local molecular contributions. Disease vulnerability was associated with enrichment for developmental processes, such as synapse formation and cell-to-cell signaling. Conversely, enrichment for immune and inflammatory mechanisms was protective. These findings suggest that interactions between neurons and their external environment may be involved in the disease pathophysiology, which we consider in more detail here.

The prominent role of cell signaling and immune functional annotations presents a potential link with the cytokine hypothesis of schizophrenia. The account posits that the pathophysiology originates from abnormal expression of cytokines (regulators of immune and in-

TABLE 1. **Summarized GO terms associated with greater brain tissue volume deformation |** GOrilla was used to identify GO terms and biological processes associated with greater deformation in schizophrenia patients. Results were summarized and subdivided into clusters using REViGO and are shown for the third parcellation resolution (i.e., 234 nodes). Cluster labels are ranked according to *P*-values. If applicable, examples of biological processes are provided for each cluster (See Table S2 for full results).

Cluster label	P-value	FDR q-value	Examples of biological process
Regulation of nervous system development	6.18E-10	3.64E-06	Regulation of cell development Regulation of neuron differentiation Regulation of neurogenesis
Regulation of localization	6.43E-09	1.89E-05	
Regulation of multicellular organismal process	6.62E-09	1.56E-05	
Regulation of cell projection organization	9.32E-09	1.83E-05	Regulation of plasma membrane bounded cell projection organization Positive regulation of cell projection organization
Regulation of developmental process	1.09E-08	1.60E-05	
System development	1.59E-08	1.87E-05	Anatomical structure development Nervous system development
Synaptic signaling	3.09E-08	3.31E-05	Trans-synaptic signaling Regulation of trans-synaptic signaling Chemical synaptic transmission
Signaling	1.28E-07	8.41E-05	
Cell-cell signaling	1.94E-07	1.20E-04	
Regulation of secretion by cell	3.04E-07	1.63E-04	Regulation of transport Regulation of secretion
MAPK cascade	8.18E-07	3.70E-04	Signal transduction by protein phosphorylation Phosphorylation
Developmental process	8.29E-07	3.62E-04	
Signal transduction	1.00E-06	4.22E-04	
Regulation of signaling	3.27E-06	1.10E-03	
Intracellular signal transduction	4.16E-06	1.32E-03	
Behaviour	4.42E-06	1.37E-03	
Regulation of cell communication	5.14E-06	1.55E-03	
Cation transmembrane transport	6.79E-06	2.00E-03	Metal ion transport Cation transport Regulation of ion transport
Cell communication	1.07E-05	2.58E-03	
Regulation of system process	2.19E-05	4.52E-03	
Regulation of small GTPase mediated signal transduction	2.33E-05	4.73E-03	
Ion transport	4.19E-05	8.23E-03	
Regulation of cellular process	5.43E-05	9.99E-03	
Regulation of GTPase activity	5.47E-05	9.91E-03	
Regulation of muscle system process	5.73E-05	1.02E-02	
Synaptic membrane adhesion	7.91E-05	1.33E-02	
Cell projection organization	8.35E-05	1.39E-02	

flammatory responses), perhaps as a result of infection [25, 38, 55, 88]. The subsequent immune response interfere with normal neurodevelopment, leading to atypical synaptic connectivity. Furthermore, the fact that brain regions with high deformation were enriched for gene sets related to regulation of nervous system development, such as neuron differentiation and cell development, is consistent the hypothesis that genes associated with schizophrenia may affect early neurodevelopmental processes [10].

TABLE 2. **Summarized GO terms associated with lower brain tissue volume deformation |** GOrilla was used to identify GO terms and biological processes associated with lower deformation in schizophrenia patients. Results were summarized and subdivided into clusters using REViGO and are shown for the third parcellation resolution (i.e., 234 nodes). Cluster labels are ranked according to *P*-values. If applicable, examples of biological processes are provided for each cluster (See Table S3 for full results).

Cluster label	P-value	FDR q-value	Examples of biological process
Immune response	4.62E-16	5.90E-12	Regulation of immune system process Leukocyte activation involved in immune response Cell activation involved in immune response
Defense response	3.15E-12	2.01E-08	
Immune system response	8.15E-12	3.47E-08	
SRP-dependent cotranslational protein targeting to membrane	1.00E-09	1.86E-06	Cotranslational protein targeting to membrane Protein targeting to ER
Detection of external biotic stimulus	1.25E-08	9.99E-06	Response to external biotic stimulus Defense response to other organism
Inflammatory response	4.16E-08	2.53E-05	Innate immune response Regulation of defense response
Humoral immune response	7.15E-08	4.15E-05	
Macrophage activation	9.73E-08	5.41E-05	
Detection of biotic stimulus	1.04E-07	5.51E-05	
Innate immune response in mucosa	1.53E-07	6.99E-05	Mucosal immune response
Regulation of cytokine biosynthetic process	2.31E-07	9.24E-05	Positive regulation of cytokine production Positive regulation of chemokine production
Cell activation	2.89E-07	1.12E-04	
Positive regulation of cell adhesion	4.50E-07	1.64E-04	Regulation of leukocyte cell-cell adhesion Regulation of cell-cell adhesion
Nuclear-transcribed mRNA catabolic process	7.029E-07	2.42E-04	mRNA catabolic process RNA catabolic process
G protein-coupled purinergic nucleotide receptor signaling pathway	7.72E-07	2.53E-04	Purinergic nucleotide receptor signaling pathway G protein-coupled purinergic receptor signaling pathway
Regulation of myeloid leukocyte differentiation	1.20E-06	3.48E-04	Regulation of osteoclast differentiation
Response to lipoprotein particle	1.41E-06	3.91E-04	
Response to biotic stimulus	2.14E-06	5.58E-04	
Cell surface receptor signaling pathway	2.33E-06	5.95E-04	
Cellular response to lipoprotein particle stimulus	4.24E-06	9.68E-04	
Very-low-density lipoprotein particle clearance	5.65E-06	1.25E-03	Very-low-density lipoprotein particle assembly
Translational initiation	7.55E-06	1.53E-03	Translation Peptide biosynthetic process
Killing of cells of other organism	2.33E-05	3.63E-03	Disruption of cells of other organism
Organic cyclic compound catabolic process	2.36E-05	3.64E-03	
Positive regulation of response to stimulus	2.59E-05	3.85E-03	
Organ or tissue specific immune response	3.11E-05	4.52E-03	
Nucleosome assembly	3.96E-05	5.44E-03	Nucleosome organization
Purinergic receptor signaling pathway	4.27E-05	5.74E-03	
Cytokine-mediated signaling pathway	5.76E-05	7.08E-03	
Response to nitrogen compound	6.25E-05	7.54E-03	
Exocytosis	7.27E-05	8.52E-03	
Phagocytosis, engulfment	7.29E-05	8.47E-03	
Regulation of myeloid leukocyte mediated immunity	7.82E-05	9.00E-03	
Protein-DNA complex subunit organization	8.95E-05	9.94E-03	

More generally, the present results build on the well-documented genetic contributions of schizophrenia. For example, Romme and colleagues demonstrated that the transcriptional profile of schizophrenia risk genes across cortical regions correlates with regional white matter disconnectivity [68]. The biological processes of highest-loading gene sets in that study had considerable overlap with those reported here, including genes associated with cell-to-cell signaling. In addition, a recent study on polygenic schizophrenia risk, using longitudinal transcriptomic read-outs *in vitro*, found patterns of differential expression in clusters related to cell signaling and synapse formation [57]. Finally, schizotypy-related cortical myelination, as assessed by MRI, has been associated with a set of genes enriched for neuronal signaling and function in a recent study in healthy young population [67]. Altogether, the present results point towards a specific set of biochemical pathways that potentially mediate tissue loss, but the precise underlying mechanism still needs to be directly tested and mapped out.

A spreading hypothesis of schizophrenia?

Our results are broadly reminiscent of an emerging literature on the signature of network structure in neurodegeneration [28, 63]. In neurodegenerative diseases, trans-neuronal transport of toxic misfolded proteins is associated with cell death and atrophy [46, 50, 87]. As a result, patterns of atrophy in neurodegenerative diseases often resemble structural and functional network patterns [16], a result that has been reported in Alzheimer's disease [39, 66, 72], Parkinson's disease [92, 95, 96] and amyotrophic lateral sclerosis [70].

Do the present results support an analogous "spreading" hypothesis of schizophrenia? We have demonstrated that connectivity and deformation (i.e., reductions in brain tissue volume, but not necessarily cell death) are related in schizophrenia, and we also find evidence that genes associated with extraneuronal signaling, synaptic plasticity and pruning are involved. Nevertheless, the evidence is circumstantial and it is impossible to disentangle the two. An alternative possibility is that systematic white matter disconnectivity - which we do not measure here - impedes normal trans-neuronal transport of trophic factors, leading to deformation among connected populations. How local gene expression and global structural and functional architecture interact remains an exciting open question [26].

Methodological considerations

We confirmed that the present results do not trivially depend on confounding factors such as parcellation resolution and spatial distance, but there are several technological factors that need to be taken into account as well. Structural connectivity, as estimated by diffusion weighted imaging, is prone to systematic false positives and false negatives [47, 79]. Connectomes generated by streamline tractography are undirected, so it is impossible to test the causal effect of connectivity on deformation. Likewise, we cannot directly measure neuronal malformation *in vivo*; we instead operationalized deformation as changes in tissue volume density. Finally, gene expression does not necessarily correlate with protein synthesis; the putative role of cell signaling and inflammation proteins in schizophrenia-related deformation needs warrants further research.

In addition, the present results are valid for a single dataset featuring chronic patients, and need to be replicated. Moreover, there is limited information available on medication history or adherence of the patients, making it difficult to assess whether medication influences the results. Our control analyses on a subset of patients indicate that the network effects reported here are unlikely to be correlated with chlorpromazine equivalent antipsychotic medication dose. Other groups have recently reported similar relationships between anatomical covariance networks and changes in cortical thickness in first-episode psychosis, chronic schizophrenia and treatment-resistant schizophrenia [86], suggesting that the observed effect is likely to be present earlier in the disease and in drug-naive patients. Finally, the current results are correlational: it is impossible to infer whether deformation drives structural and/or functional disconnectivity reported in previous literature or vice versa, or whether there is another underlying mechanism that independently potentiates both tissue loss and disconnectivity [29, 32, 68, 69]. Application of the present methodology to longitudinal samples will help to resolve the temporal evolution of these effects.

Summary

The present study demonstrates that schizophrenia-related deformation is linked to the structural and functional network organization of the brain. The relationship may be promoted by local transcriptional factors involved in signaling and immune function. Altogether, these results point to a confluence of local and global factors in shaping neurodegeneration in schizophrenia.

MATERIALS and METHODS

NUSDAST dataset

Data were derived using the Northwestern University Schizophrenia Data and Software Tool (NUSDAST) [42], which was obtained from XNAT Central (http://central.xnat.org/) and the SchizConnect data sharing portal (http://schizconnect.org/). The NUSDAST dataset is a cohort of individuals with schizophrenia, their non-psychotic siblings, healthy controls and their siblings. Detailed information about the NUSDAST dataset and the data collection procedure is available at [42].

We obtained 1.5 T T1-weighted MRI scans for the baseline visit of schizophrenia patients and healthy con-

trols from the NUSDAST database. Participants with failed MRI processing quality control were removed (See *Neuroimaging data analysis*) and data from 133 individuals with schizophrenia (48 female, 34.7±12.9 years) and 113 healthy controls (64 female, 23.5±8.4 years) was used for further analyses. To assess the severity of the disease in patients with schizophrenia, we calculated scores from the Scale for the Assessment of Positive Symptoms (SAPS; [3]) and the Scale for the Assessment of Negative Symptoms (SANS; [2]), two widely used schizophrenia symptom rating scales. Following the method described in [81], we generated a composite (i.e., total) and a global (i.e., summary) score for SANS and SAPS ratings. SANS scores reflect symptoms of affective flattening, alogia, avolition, anhedonia, and attention; SAPS scores reflect symptoms of hallucinations, delusions, bizarre behaviour, and thought disorder. The SAPS composite and global scores were 18.64 ± 14.53 and 5.03 ± 3.10, respectively. The SANS composite and global scores were 24.18 ± 15.17 and 9.04 ± 4.55, respectively.

Neuroimaging data analysis

The baseline T1-weighted MRI scans of schizophrenia patients and healthy controls were obtained from the NUSDAST dataset. Details about the neuroimaging data acquisition are provided by Kogan and colleagues at [42]. Briefly, all MRI scans were acquired on the same 1.5 T Vision scanner platform (Siemens Medical Systems) at the Mallinckrodt Institute of Radiology at Washington University School of Medicine; data acquisition parameters are available in detail at [42]. Automated pre-processing was performed using the *minc-bpipe-library* pipeline (https://github.com/CobraLab/minc-bpipe-library) on each T1-weighted MRI scan. The outputs were visually inspected and quality-controlled, resulting in the removal of 8 participants due to failure in processing. A group-average template for the remaining participants, both healthy controls and patients, was built using the ANTs multivariate template construction tool (https://github.com/CobraLab/documentation/wiki/ANTs-Multivariate-Template-Construction).

Deformation-Based Morphometry (DBM)

Local changes in brain tissue volume density were calculated using deformation-based morphometry (DBM). Regional DBM values can be considered as measures of tissue loss (termed as *deformation* in this manuscript) or tissue expansion [14, 17, 45, 76, 95]. DBM values are estimated from the deformation applied to each voxel to non-linearly register each brain to a standard template. In the present study, we used ANTs multivariate template construction pipeline [5] (*antsMultivariateTemplateConstruction2.sh*) to measure the DBM values. We first calculated a study-specific brain template using T1-weighted scans of both schizophrenia patients and healthy controls. Using an affine transformation and a non-linear warp, the T1 image of each subject was registered to the group template. Following the non-linear transformation of each structural brain image to the template image during the registration process, a deformation based map was generated for each subject in the template space. A deformation map shows the amount of displacement of each voxel in each direction in the 3-dimensional template space that was required to transform each brain image from subject to template space. The local change in tissue density is then estimated as the derivative of the displacement of a given voxel in each direction. The derivatives can be calculated as the determinant of the Jacobian matrix of displacement, $\mathbf{J}$, which is given as [95]:

$$J = \frac{\partial U}{\partial x} = \begin{bmatrix} \frac{\partial u_1}{\partial x_1} & \frac{\partial u_1}{\partial x_2} & \frac{\partial u_1}{\partial x_3} \\ \frac{\partial u_2}{\partial x_1} & \frac{\partial u_2}{\partial x_2} & \frac{\partial u_2}{\partial x_3} \\ \frac{\partial u_3}{\partial x_1} & \frac{\partial u_3}{\partial x_2} & \frac{\partial u_3}{\partial x_3} \end{bmatrix} \tag{1}$$

where $x = (x_1, x_2, x_3)$ is a position in a given T1-weighted image at the subject space, which is then transformed to the template space in each direction using the displacement given by the vectors $\mathbf{U} = (\mathbf{u_1}, \mathbf{u_2}, \mathbf{u_3})$. Each element of the Jacobian matrix is estimated using a first order approximation. As an example, J_{13} can be calculated as following:

$$\frac{\partial u_1}{\partial x_3} = \frac{u_1(x_1, x_2, x_3 + \delta) - u_1(x_1, x_2, x_3 - \delta)}{2\delta} \tag{2}$$

where δ is the position of a given voxel along axis x_3. Then, the local changes in tissue density were calculated as the determinant of the Jacobian matrix; such that no change in volume is given with 1 (i.e., no displacement relative to template), tissue expansion is given with a value between 0 and 1 (i.e., subject image was shrunk to be transformed to template space), and tissue loss or deformation is given with a value larger than 1 (i.e., subject image was expanded to be transformed to template space). For easier interpretation of the changes in volume density, we calculated the logarithm of the determinant, such that no change is given by 0, tissue loss (i.e., deformation) is given by a positive value, and tissue expansion is given by a negative value.

Finally, the deformation maps were blurred (2 mm full-width/half-maximum) and the non-brain tissue was removed from each brain using FreeSurfer image analysis suite (release v6.0.0; documented and freely available for download at http://surfer.nmr.mgh.harvard.edu/). The voxel-wise data was then extracted for each participant for further analysis.

Regional brain deformation

We defined schizophrenia-related deformation patterns as the differences between the deformation maps of

schizophrenia patients and healthy controls by simply contrasting the deformation maps of the 2 groups. More specifically, we used a two-tailed two-sample t-test of voxel-wise differences between DBM values of patients and controls, while controlling for age, to assess the group effect on deformation maps. T-statistics were converted to z-statistics, where a larger positive z-score corresponds to greater deformation in patients compared to healthy controls. Benjamini-Hochberg procedure [7] was used to correct for multiple comparisons by controlling the false discovery rate (FDR) at 5% across all voxels.

Network reconstruction

Anatomical atlas. The brain was parcellated into 83 cortical and subcortical areas according to the Desikan-Killiany atlas [19], which is an automated labeling system where nodes are defined based on anatomical landmarks. The parcells were then further subdivided into 129, 234, 463 and 1015 approximately equally sized parcels according to the Lausanne anatomical atlas following the method proposed by Cammoun and colleagues [13]. The deformation value of each parcel was estimated as the mean z-score of all the voxels assigned to that parcel. All 5 parcellation resolutions were used to ensure that the observed effects are independent of spatial scale.

Healthy structural and functional networks. Structural and functional connectivity data, collected from 70 healthy individuals at Lausanne University Hospital in Switzerland (age 28.8 ± 9.1 years, 27 females) on a 3 T scanner and described in detail in a previous study by Mišić and colleagues [54], was used to construct high-quality reference brain networks of healthy population. In brief, deterministic streamline tractography was used to construct structural connectivity matrices for each healthy individual from their diffusion spectrum imaging (DSI) data at each of the five parcellation resolutions. Each pair-wise structural connection was weighted by fiber density. In order to correct for any size differences between the two brain areas as well as the inherent bias towards longer fibers in tractography process, the fiber density of structural connections was estimated as the number of streamlines normalized by the mean surface area of the two regions and the mean length of streamlines connecting them [35, 54]. Finally, a binary group-average structural connectivity matrix was generated using a consensus approach preserving the edge length distribution in individual participants [8, 9, 53, 54].

Furthermore, functional data was collected for the same 70 participants using eyes-open resting-state functional MRI (rs-fMRI) scans and was pre-processed as described in [54]. Functional connectivity between pairs of brain regions was estimated as zero-lag Pearson correlation coefficient between rs-fMRI time series of the two regions for each individual at each parcellation resolution. The group-average functional connectivity matrix was estimated as the mean connectivity of pair-wise connections across individuals. We retained negative functional connections for the original analyses reported in the main text. However, we repeated the analyses after thresholding the negative connections (i.e., assigning them to zero) to rule out the possibility of any confounding effects. The results remained the same when we removed the negative functional connections both at the individual subject level and at the group-average level.

Neighbourhood deformation estimates. We used the above structural and functional connectivity networks as the underlying architecture to estimate the deformation values of the structurally- and functionally-defined neighbours of each brain region. The collective deformation of structural neighbours of i-th brain region (D_i) was estimated as the mean deformation of all the brain regions that are connected to node i by an underlying structural connection:

$$D_i = \frac{1}{N}\sum_{j=1}^{N} d_j \tag{3}$$

where D_i is collective deformation of structural neighbours of i-th node, d is node deformation, and N is the total number of nodes that are connected to node i with a structural connection in the group-level structural connectivity network. The correction term $1/N$ was added to normalize the sum by the number of connections (i.e., correcting for node degree). Therefore, for each node, a single value was estimated as the mean deformation of its neighbours. Finally, a correlation coefficient was calculated between the deformation of all nodes and the mean deformation of their neighbours.

The collective deformation of functional neighbours of node i (D_i) was estimated in an analogous manner, but the deformation values of the neighbours were weighted by the strength of functional correlations:

$$D_i = \frac{1}{N}\sum_{j=1}^{N} d_j \times FC_{ij} \tag{4}$$

where D_i is collective deformation of functionally-defined neighbours of i-th node, d is node deformation, N is the number of the nodes that are directly connected to node i with a structural connection in the group-level structural connectivity matrix, and FC_{ij} is the mean functional connectivity between nodes i and j across individuals. Similar to the above procedure, the deformation values of all nodes were correlated with the collective deformation values of their neighbours weighted by functional connectivity and a correlation coefficient was calculated.

In addition, a multiple linear regression model (*fitlm.m* function from MATLAB R2017b) was used to simultaneously include both structurally- and functionally- defined means of neighbours' deformation estimates as predictors of node deformation. We used the adjusted correlation coefficient to assess the relationship between deformation values of the nodes and their neighbours. All the above analyses were repeated at all 5 parcellation resolutions.

Microarray expression data processing

Regional microarray expression data were obtained from six post-mortem brains provided by the Allen Human Brain Atlas (http://human.brain-map.org/) [37]. These data were processed and mapped to parcellated brain regions (from 83 to 1015 nodes according to Lausanne anatomical atlas [13]; see *Anatomical atlas*) using the abagen toolbox (https://github.com/netneurolab/abagen).

Briefly, genetic probes were filtered based on their intensity relative to background noise levels [65]; probes with intensity less than background in ≥50% of samples were discarded. A single probe with the highest differential stability, $\Delta_S(p)$, was selected to represent each gene [36], where differential stability was calculated as:

$$\Delta_S(p) = \frac{1}{\binom{N}{2}} \sum_{i=1}^{N-1} \sum_{j=i+1}^{N} \rho[B_i(p), B_j(p)] \tag{5}$$

Here, ρ is Spearman's rank correlation of the expression of a single probe p across regions in two donor brains, B_i and B_j, and N is the total number of donor brains. This procedure retained 20,597 probes, each representing a unique gene.

Next, samples were assigned to brain regions using their corrected MNI coordinates (https://github.com/chrisfilo/alleninf) by finding the nearest region, up to 2mm away. To reduce the potential for misassignment, sample-to-region matching was constrained by hemisphere and cortical/subcortical divisions [4]. If a brain region was not assigned any sample based on the above procedure, the sample closest to the centroid of that region was selected in order to ensure that all brain regions were assigned a value.

Samples assigned to the same brain region were averaged separately for each donor. Gene expression values were then normalized separately for each donor across regions using a scaled robust sigmoid function [33]:

$$x_{norm} = \frac{1}{1 + \exp(-\frac{(x_g - \langle x_g \rangle)}{\sigma_g})} \tag{6}$$

where $\langle x_g \rangle$ is the median and σ_g is the standard deviation of the expression value of a single gene across regions. Normalized gene expression values were then rescaled to a unit interval:

$$x_{scaled} = \frac{x_{norm} - \min(x_{norm})}{\max(x_{norm}) - \min(x_{norm})} \tag{7}$$

Scaled expression profiles were finally averaged across donors, resulting in a single matrix $\mathbf{G}$ with r rows corresponding to brain regions and g columns corresponding to the retained 20,597 genes. It should be noted that while this procedure was repeated separately for all parcellation resolutions, the highest resolutions were limited by the spatial coverage of available samples in the donor brains. Because of this limitation, estimated microarray expression data is likely to be unreliable at these scales.

Gene ontology analysis

Multivariate partial least squares (PLS) analysis was used to statistically assess the relationship between microarray expression data and regional brain deformation [52, 83, 89]. PLS analysis is a multivariate statistical technique that identifies weighted patterns of variables in two sets of data that maximally covary with each other [43, 51, 52]. In the present study, we submitted parcellated brain deformation, $\mathbf{X}$, and gene expression data, $\mathbf{Y}$, to PLS to construct a linear combination of genes associated with regional variance in grey matter deformation. A correlation matrix ($\mathbf{X}'\mathbf{Y}$) was computed from the normalized data, which was then subjected to a singular value decomposition (SVD) [21], as following:

$$\mathbf{R} = \mathbf{X}'\mathbf{Y} = \mathbf{USV}' \tag{8}$$

The decomposition results in two orthonormal matrices of left and right singular vectors ($\mathbf{U}$ and $\mathbf{V}$, respectively), and a diagonal matrix of singular values ($\mathbf{S}$). The main results of the analysis are represented as latent variables, which are constructed from the 3 resulting matrices (i.e., $\mathbf{U}$, $\mathbf{V}$, and $\mathbf{S}$). More specifically, latent variables are mutually orthogonal, weighted linear combinations of the original variables (i.e., $\mathbf{X}$ and $\mathbf{Y}$) and express the shared information between the datasets with maximum covariance. Latent variable i (LV_i) is composed of the ith column vector of $\mathbf{U}$, ith column vector of $\mathbf{V}$, and the ith singular value from $\mathbf{S}$. The elements of the column vectors of $\mathbf{U}$ and $\mathbf{V}$ are the weights of the original brain deformation values and gene expression profiles, respectively, that contribute to the latent variable. The weighted deformation and gene expression patterns maximally covary with each other, and the covariance between them is reflected in the corresponding singular values from the diagonal elements of matrix $\mathbf{S}$.

We used permutation testing to assess the significance of the relationship between the two data blocks [24]. During each permutation, the rows of data matrix $\mathbf{X}$ were reordered randomly and a new, permuted, correlation matrix was calculated from $\mathbf{Y}$ and permuted $\mathbf{X}$. Similar to the original analysis, the permuted correlation matrix was then subjected to SVD. The procedure was repeated 1,000 times resulting in a null distribution of singular values. To test the null hypothesis that there is no specific relationship between microarray expression data and regional brain deformation, a P-value was estimated for each latent variable as the proportion of the times that the permuted singular values were greater than or equal to the original singular value. The analysis was repeated for the first 3 parcellation resolutions (83, 129,

and 234 nodes) since the microarray expression data can be estimated with higher reliability for these resolutions compared to finer ones (See *Microarray expression data processing*).

For each resolution, the resulting loadings from the PLS model were split into positive and negative values, indicating the genes that are positively and negatively correlated with higher deformation. Gene lists were ranked based on the values of PLS-derived loadings (the negative loadings were ranked inversely from more negative to less negative, indicating higher to lower anti-correlation with deformation).

The two ranked lists of genes were separately submitted to an online gene ontology (GO) enrichment analysis tool, GOrilla (http://cbl-gorilla.cs.technion.ac.il, version Octover 06, 2018) [22, 23], to identify the enriched GO terms that correspond to the top ranked genes from each of the two lists [89]. GOrilla database includes 11,778 GO terms that are used for the enrichment analysis. In the advanced parameter settings of GOrilla, we set the P-value threshold to 10^{-4} and unchecked the "Run GOrilla in fast mode" option. GOrilla applies an FDR correction to the resulting P-values to correct for multiple comparisons of the total 11,778 GO terms in its database, using the Benjamini-Hochberg method [7].

We used another online tool, REViGO (http://revigo.irb.hr/) [77], to summarize the lists of resulting GO terms from GOrilla analysis. REViGO summarizes the gene ontology terms by constructing subgroups of redundant terms based on semantic similarity of a given term to other terms in the whole list as well as the provided P-values [77]. We set the "Allowed similarity" to 0.5 in the parameter space of REViGO to generate a relatively small list of clusters (i.e., subgroups) of GO terms for visualization purposes.

ACKNOWLEDGMENTS and DISCLOSURES

This research was undertaken thanks in part to funding from the Canada First Research Excellence Fund, awarded to McGill University for the Healthy Brains for Healthy Lives initiative. BM acknowledges support from the Natural Sciences and Engineering Research Council of Canada (NSERC Discovery Grant RGPIN #017-04265) and from the Fonds de Recherche du Québec - Santé (FRSQ, Chercheur Boursier). GS acknowledges support from the Natural Sciences and Engineering Research Council of Canada (NSERC) and from the Healthy Brains for Healthy Lives (HBHL) initiative at McGill University. CM acknowledges support from the Canadian Institutes of Health Research (CIHR) and from the Healthy Brains for Healthy Lives (HBHL) initiative at McGill University. PH acknowledges Swiss National Science Foundation grant #156874. ML acknowledges support from the Canadian Institutes of Health Research (CIHR, 68961). ML has received a Salary award from the Fonds de Recherche du Québec - Santé (FRSQ) and a James McGill Professorship. ML reports grants from Otsuka Lundbeck Alliance, personal fees from Otsuka Canada, personal fees from Lundbeck Canada, grants and personal fees from Janssen, and personal fees from MedAvante-Prophase, outside the submitted work. The authors report no other biomedical financial interests or potential conflicts of interest.

The authors thank Dr. Alessandra Griffa for data collection and processing of healthy structural and functional networks and providing insightful comments on the manuscript. The authors also thank Dr. Andrew Zalesky for providing insightful comments and feedback on the manuscript and Dr. František Váša for sharing the von Economo cytoarchitectonic atlases.

[1] Allman, J. M., Tetreault, N. A., Hakeem, A. Y., Manaye, K. F., Semendeferi, K., Erwin, J. M., Park, S., Goubert, V., and Hof, P. R. (2010). The von economo neurons in frontoinsular and anterior cingulate cortex in great apes and humans. *Brain Struct Funct*, 214(5-6):495–517.

[2] Andreasen, N. C. et al. (1983). *The Scale for the Assessment of Negative Symptoms (SANS)*. University of Iowa Iowa City.

[3] Andreasen, N. C. et al. (1984). *Scale for the assessment of positive symptoms (SAPS)*. University of Iowa Iowa City.

[4] Arnatkeviciute, A., Fulcher, B. D., and Fornito, A. (2018). A practical guide to linking brain-wide gene expression and neuroimaging data. *bioRxiv*, page 380089.

[5] Avants, B. B., Tustison, N. J., Song, G., Cook, P. A., Klein, A., and Gee, J. C. (2011). A reproducible evaluation of ants similarity metric performance in brain image registration. *Neuroimage*, 54(3):2033–2044.

[6] Avena-Koenigsberger, A., Misic, B., and Sporns, O. (2018). Communication dynamics in complex brain networks. *Nat Rev Neurosci*, 19(1):17.

[7] Benjamini, Y. and Hochberg, Y. (1995). Controlling the false discovery rate: a practical and powerful approach to multiple testing. *Journal of the royal statistical society. Series B (Methodological)*, pages 289–300.

[8] Betzel, R. F., Avena-Koenigsberger, A., Goñi, J., He, Y., De Reus, M. A., Griffa, A., Vértes, P. E., Mišic, B., Thiran, J.-P., Hagmann, P., et al. (2016). Generative models of the human connectome. *Neuroimage*, 124:1054–1064.

[9] Betzel, R. F., Griffa, A., Hagmann, P., and Mišić, B. (2018). Distance-dependent consensus thresholds for generating group-representative structural brain networks. *Network Neuroscience*, pages 1–22.

[10] Birnbaum, R. and Weinberger, D. R. (2017). Genetic insights into the neurodevelopmental origins of schizophrenia. *Nature Reviews Neuroscience*, 18(12):727.

[11] Brandl, F., Avram, M., Weise, B., Shang, J., Simões, B., Bertram, T., Ayala, D. H., Penzel, N., Gürsel, D. A., Bäuml, J., et al. (2018). Specific substantial dysconnectivity in schizophrenia a transdiagnostic multimodal meta-analysis of resting-state functional and structural mri studies. *Biological Psychiatry*.

[12] Brüne, M., Schöbel, A., Karau, R., Benali, A., Faustmann, P. M., Juckel, G., and Petrasch-Parwez, E. (2010). Von economo neuron density in the anterior cingulate cortex is reduced in early onset schizophrenia. *Acta Neuropathologica*, 119(6):771–778.

[13] Cammoun, L., Gigandet, X., Meskaldji, D., Thiran, J. P., Sporns, O., Do, K. Q., Maeder, P., Meuli, R., and Hagmann, P. (2012). Mapping the human connectome at multiple scales with diffusion spectrum mri. *Journal of neuroscience methods*, 203(2):386–397.

[14] Cardenas, V. A., Boxer, A. L., Chao, L. L., Gorno-Tempini, M. L., Miller, B. L., Weiner, M. W., and Studholme, C. (2007). Deformation-based morphometry reveals brain atrophy in frontotemporal dementia. *Archives of Neurology*, 64(6):873–877.

[15] Cauda, F., Geminiani, G. C., and Vercelli, A. (2014). Evolutionary appearance of von economoâĂŹs neurons in the mammalian cerebral cortex. *Front Hum Neurosci*, 8:104.

[16] Cauda, F., Nani, A., Manuello, J., Premi, E., Palermo, S., Tatu, K., Duca, S., Fox, P. T., and Costa, T. (2018). Brain structural alterations are distributed following functional, anatomic and genetic connectivity. *Brain*, 141(11):3211–3232.

[17] Chung, M., Worsley, K., Paus, T., Cherif, C., Collins, D., Giedd, J., Rapoport, J., and Evans, A. (2001). A unified statistical approach to deformation-based morphometry. *NeuroImage*, 14(3):595–606.

[18] Cropley, V. L., Klauser, P., Lenroot, R. K., Bruggemann, J., Sundram, S., Bousman, C., Pereira, A., Di Biase, M. A., Weickert, T. W., Weickert, C. S., et al. (2016). Accelerated gray and white matter deterioration with age in schizophrenia. *Am J Psychiatry*, 174(3):286–295.

[19] Desikan, R. S., Ségonne, F., Fischl, B., Quinn, B. T., Dickerson, B. C., Blacker, D., Buckner, R. L., Dale, A. M., Maguire, R. P., Hyman, B. T., et al. (2006). An automated labeling system for subdividing the human cerebral cortex on mri scans into gyral based regions of interest. *Neuroimage*, 31(3):968–980.

[20] Di Biase, M. A., Cropley, V. L., Cocchi, L., Fornito, A., Calamante, F., Ganella, E. P., Pantelis, C., and Zalesky, A. (2018). Linking cortical and connectional pathology in schizophrenia. *Schiz Bull*.

[21] Eckart, C. and Young, G. (1936). The approximation of one matrix by another of lower rank. *Psychometrika*, 1(3):211–218.

[22] Eden, E., Lipson, D., Yogev, S., and Yakhini, Z. (2007). Discovering motifs in ranked lists of dna sequences. *PLoS computational biology*, 3(3):e39.

[23] Eden, E., Navon, R., Steinfeld, I., Lipson, D., and Yakhini, Z. (2009). Gorilla: a tool for discovery and visualization of enriched go terms in ranked gene lists. *BMC bioinformatics*, 10(1):48.

[24] Edgington, E. and Onghena, P. (2007). *Randomization tests*. Chapman and Hall/CRC.

[25] Fatemi, S. H. and Folsom, T. D. (2009). The neurodevelopmental hypothesis of schizophrenia, revisited. *Schiz Bull*, 35(3):528–548.

[26] Fornito, A., Arnatkeviciute, A., and Fulcher, B. (2018). Bridging the gap between transcriptome and connectome. *OSF Preprints. August*, 24.

[27] Fornito, A., Yücel, M., Patti, J., Wood, S., and Pantelis, C. (2009). Mapping grey matter reductions in schizophrenia: an anatomical likelihood estimation analysis of voxel-based morphometry studies. *Schizophrenia Res*, 108(1-3):104–113.

[28] Fornito, A., Zalesky, A., and Breakspear, M. (2015). The connectomics of brain disorders. *Nat Rev Neurosci*, 16(3):159.

[29] Fornito, A., Zalesky, A., Pantelis, C., and Bullmore, E. T. (2012). Schizophrenia, neuroimaging and connectomics. *Neuroimage*, 62(4):2296–2314.

[30] Friedrichs-Maeder, C. L., Griffa, A., Schneider, J., Hüppi, P. S., Truttmann, A., and Hagmann, P. (2017). Exploring the role of white matter connectivity in cortex maturation. *PloS one*, 12(5):e0177466.

[31] Fries, P. (2015). Rhythms for cognition: communication through coherence. *Neuron*, 88(1):220–235.

[32] Friston, K. J. and Frith, C. D. (1995). Schizophrenia: a disconnection syndrome. *Clin Neurosci*, 3(2):89–97.

[33] Fulcher, B. D. and Fornito, A. (2016). A transcriptional signature of hub connectivity in the mouse connectome. *Proceedings of the National Academy of Sciences*, 113(5):1435–1440.

[34] Goodkind, M., Eickhoff, S. B., Oathes, D. J., Jiang, Y., Chang, A., Jones-Hagata, L. B., Ortega, B. N., Zaiko, Y. V., Roach, E. L., Korgaonkar, M. S., et al. (2015). Identification of a common neurobiological substrate for mental illness. *JAMA Psychiat*, 72(4):305–315.

[35] Hagmann, P., Cammoun, L., Gigandet, X., Meuli, R., Honey, C. J., Wedeen, V. J., and Sporns, O. (2008). Mapping the structural core of human cerebral cortex. *PLoS biology*, 6(7):e159.

[36] Hawrylycz, M., Miller, J. A., Menon, V., Feng, D., Dolbeare, T., Guillozet-Bongaarts, A. L., Jegga, A. G., Aronow, B. J., Lee, C.-K., Bernard, A., et al. (2015). Canonical genetic signatures of the adult human brain. *Nature neuroscience*, 18(12):1832.

[37] Hawrylycz, M. J., Lein, E. S., Guillozet-Bongaarts, A. L., Shen, E. H., Ng, L., Miller, J. A., Van De Lagemaat, L. N., Smith, K. A., Ebbert, A., Riley, Z. L., et al. (2012). An anatomically comprehensive atlas of the adult human brain transcriptome. *Nature*, 489(7416):391.

[38] Howes, O. and McCutcheon, R. (2017). Inflammation and the neural diathesis-stress hypothesis of schizophrenia: a reconceptualization. *Trans Psychiat*, 7(2):e1024.

[39] Iturria-Medina, Y., Sotero, R. C., Toussaint, P. J., Evans, A. C., Initiative, A. D. N., et al. (2014). Epidemic spreading model to characterize misfolded proteins propagation in aging and associated neurodegenerative disorders. *PLoS Comput Biol*, 10(11):e1003956.

[40] Jucker, M. and Walker, L. C. (2018). Propagation and spread of pathogenic protein assemblies in neurodegenerative diseases. *Nat Neurosci*, 21(10):1341.

[41] Kasai, K., Shenton, M. E., Salisbury, D. F., Hirayasu, Y., Lee, C.-U., Ciszewski, A. A., Yurgelun-Todd, D., Kikinis, R., Jolesz, F. A., and McCarley, R. W. (2003). Progressive decrease of left superior temporal gyrus gray matter volume in patients with first-episode schizophrenia. *American Journal of Psychiatry*, 160(1):156–164.

[42] Kogan, A., Alpert, K., Ambite, J. L., Marcus, D. S., and Wang, L. (2016). Northwestern university schizophrenia data sharing for schizconnect: A longitudinal dataset for large-scale integration. *NeuroImage*, 124:1196–1201.

[43] Krishnan, A., Williams, L. J., McIntosh, A. R., and Abdi, H. (2011). Partial least squares (pls) methods for neuroimaging: a tutorial and review. *Neuroimage*, 56(2):455–475.

[44] Kuperberg, G. R., Broome, M. R., McGuire, P. K., David, A. S., Eddy, M., Ozawa, F., Goff, D., West, W. C., Williams, S. C., van der Kouwe, A. J., et al. (2003). Regionally localized thinning of the cerebral cortex in schizophrenia. *Arch Gen Psychiatry*, 60(9):878–888.

[45] Leow, A. D., Klunder, A. D., Jack Jr, C. R., Toga, A. W., Dale, A. M., Bernstein, M. A., Britson, P. J., Gunter, J. L., Ward, C. P., Whitwell, J. L., et al. (2006). Longitudinal stability of mri for mapping brain change using tensor-based morphometry. *Neuroimage*, 31(2):627–640.

[46] Luk, K. C., Kehm, V., Carroll, J., Zhang, B., OâĂŹBrien, P., Trojanowski, J. Q., and Lee, V. M.-Y. (2012). Pathological α-synuclein transmission initiates parkinson-like neurodegeneration in nontransgenic mice. *Science*, 338(6109):949–953.

[47] Maier-Hein, K. H., Neher, P. F., Houde, J.-C., Côté, M.-A., Garyfallidis, E., Zhong, J., Chamberland, M., Yeh, F.-C., Lin, Y.-C., Ji, Q., et al. (2017). The challenge of mapping the human connectome based on diffusion tractography. *Nat Commun*, 8(1):1349.

[48] Makowski, C., Lewis, J. D., Lepage, C., Malla, A. K., Joober, R., Lepage, M., and Evans, A. C. (2019). Structural associations of cortical contrast and thickness in first episode psychosis. *Cerebral Cortex*.

[49] Maslov, S. and Sneppen, K. (2002). Specificity and stability in topology of protein networks. *Science*, 296(5569):910–913.

[50] Masuda-Suzukake, M., Nonaka, T., Hosokawa, M., Oikawa, T., Arai, T., Akiyama, H., Mann, D. M., and Hasegawa, M. (2013). Prion-like spreading of pathological α-synuclein in brain. *Brain*, 136(4):1128–1138.

[51] McIntosh, A. R. and Lobaugh, N. J. (2004). Partial least squares analysis of neuroimaging data: applications and advances. *Neuroimage*, 23:S250–S263.

[52] McIntosh, A. R. and Mišić, B. (2013). Multivariate statistical analyses for neuroimaging data. *Annual review of psychology*, 64:499–525.

[53] Mišić, B., Betzel, R. F., Griffa, A., de Reus, M. A., He, Y., Zuo, X.-N., van den Heuvel, M. P., Hagmann, P., Sporns, O., and Zatorre, R. J. (2018). Network-based asymmetry of the human auditory system. *Cereb Cortex*, 28(7):2655–2664.

[54] Mišić, B., Betzel, R. F., Nematzadeh, A., Goni, J., Griffa, A., Hagmann, P., Flammini, A., Ahn, Y.-Y., and Sporns, O. (2015). Cooperative and competitive spreading dynamics on the human connectome. *Neuron*, 86(6):1518–1529.

[55] Monji, A., Kato, T., and Kanba, S. (2009). Cytokines and schizophrenia: Microglia hypothesis of schizophrenia. *Psychiat Clin Neurosci*, 63(3):257–265.

[56] Mørch-Johnsen, L., Nesvåg, R., Jørgensen, K. N., Lange, E. H., Hartberg, C. B., Haukvik, U. K., Kompus, K., Westerhausen, R., Osnes, K., Andreassen, O. A., et al. (2016). Auditory cortex characteristics in schizophrenia: associations with auditory hallucinations. *Schizophrenia bulletin*, 43(1):75–83.

[57] Ori, A. P., Bot, M. H., Molenhuis, R. T., Loohuis, L. M. O., and Ophoff, R. A. (2018). A longitudinal model of human neuronal differentiation for functional investigation of schizophrenia polygenic risk. *Biol Psychiat*.

[58] Palaniyappan, L., Das, T. K., Winmill, L., Hough, M., James, A., and Palaniyappan, L. (2019). Progressive post-onset reorganisation of mri-derived cortical thickness in adolescents with schizophrenia. *Schiz Res*.

[59] Palaniyappan, L. and Liddle, P. F. (2012). Does the salience network play a cardinal role in psychosis? an emerging hypothesis of insular dysfunction. *J Psychiat Neurosci*.

[60] Palaniyappan, L., Simmonite, M., White, T. P., Liddle, E. B., and Liddle, P. F. (2013). Neural primacy of the salience processing system in schizophrenia. *Neuron*, 79(4):814–828.

[61] Patel, M. X., Arista, I. A., Taylor, M., and Barnes, T. R. (2013). How to compare doses of different antipsychotics: a systematic review of methods. *Schiz Res*, 149(1-3):141–148.

[62] Paus, T., Pesaresi, M., and French, L. (2014). White matter as a transport system. *Neuroscience*, 276:117–125.

[63] Pievani, M., Filippini, N., Van Den Heuvel, M. P., Cappa, S. F., and Frisoni, G. B. (2014). Brain connectivity in neurodegenerative diseases - from phenotype to proteinopathy. *Nat Rev Neurol*, 10(11):620.

[64] Power, J. D., Cohen, A. L., Nelson, S. M., Wig, G. S., Barnes, K. A., Church, J. A., Vogel, A. C., Laumann, T. O., Miezin, F. M., Schlaggar, B. L., et al. (2011). Functional network organization of the human brain. *Neuron*, 72(4):665–678.

[65] Quackenbush, J. (2002). Microarray data normalization and transformation. *Nature Genetics*, 32:496.

[66] Raj, A., Kuceyeski, A., and Weiner, M. (2012). A network diffusion model of disease progression in dementia. *Neuron*, 73(6):1204–1215.

[67] Romero-Garcia, R., Seidlitz, J., Whitaker, K. J., Morgan, S. E., Fonagy, P., Dolan, R. J., Jones, P. B., Goodyer, I. M., Suckling, J., , Vertes, P. E., and Bullmore, E. T. (2018). Schizotypy-related magnetization of cortex in healthy adolescence is co-located with expression of schizophrenia risk genes. *bioRxiv*.

[68] Romme, I. A., de Reus, M. A., Ophoff, R. A., Kahn, R. S., and van den Heuvel, M. P. (2017). Connectome disconnectivity and cortical gene expression in patients with schizophrenia. *Biol Psychiat*, 81(6):495–502.

[69] Rubinov, M. and Bassett, D. S. (2011). Emerging evidence of connectomic abnormalities in schizophrenia. *Journal of Neuroscience*, 31(17):6263–6265.

[70] Schmidt, R., de Reus, M. A., Scholtens, L. H., van den Berg, L. H., and van den Heuvel, M. P. (2016). Simulating disease propagation across white matter connectome reveals anatomical substrate for neuropathology staging in amyotrophic lateral sclerosis. *NeuroImage*, 124:762–769.

[71] Scholtens, L. H., de Reus, M. A., de Lange, S. C., Schmidt, R., and van den Heuvel, M. P. (2018). An mri von economo–koskinas atlas. *NeuroImage*, 170:249–256.

[72] Seeley, W. W., Crawford, R. K., Zhou, J., Miller, B. L., and Greicius, M. D. (2009). Neurodegenerative diseases target large-scale human brain networks. *Neuron*, 62(1):42–52.

[73] Sha, Z., Wager, T. D., Mechelli, A., and He, Y. (2018). Common dysfunction of large-scale neurocognitive networks across psychiatric disorders. *Biological Psychiatry*.

[74] Skudlarski, P., Jagannathan, K., Anderson, K., Stevens, M. C., Calhoun, V. D., Skudlarska, B. A., and Pearlson, G. (2010). Brain connectivity is not only lower but different in schizophrenia: a combined anatomical and functional approach. *Biol Psychiat*, 68(1):61–69.

[75] Steen, R. G., Mull, C., Mcclure, R., Hamer, R. M., and

Lieberman, J. A. (2006). Brain volume in first-episode schizophrenia: systematic review and meta-analysis of magnetic resonance imaging studies. *Br J Psychiatry*, 188(6):510–518.

[76] Studholme, C., Cardenas, V., Blumenfeld, R., Schuff, N., Rosen, H., Miller, B., and Weiner, M. (2004). Deformation tensor morphometry of semantic dementia with quantitative validation. *Neuroimage*, 21(4):1387–1398.

[77] Supek, F., Bošnjak, M., Škunca, N., and Šmuc, T. (2011). Revigo summarizes and visualizes long lists of gene ontology terms. *PloS one*, 6(7):e21800.

[78] Takahashi, T., Wood, S. J., Yung, A. R., Soulsby, B., McGorry, P. D., Suzuki, M., Kawasaki, Y., Phillips, L. J., Velakoulis, D., and Pantelis, C. (2009). Progressive gray matter reduction of the superior temporal gyrus during transition to psychosis. *Arch Gen Psychiatry*, 66(4):366–376.

[79] Thomas, C., Frank, Q. Y., Irfanoglu, M. O., Modi, P., Saleem, K. S., Leopold, D. A., and Pierpaoli, C. (2014). Anatomical accuracy of brain connections derived from diffusion mri tractography is inherently limited. *Proc Natl Acad Sci USA*, 111(46):16574–16579.

[80] van Erp, T. G., Hibar, D. P., Rasmussen, J. M., Glahn, D. C., Pearlson, G. D., Andreassen, O. A., Agartz, I., Westlye, L. T., Haukvik, U. K., Dale, A. M., et al. (2016). Subcortical brain volume abnormalities in 2028 individuals with schizophrenia and 2540 healthy controls via the enigma consortium. *Molecular psychiatry*, 21(4):547.

[81] Van Erp, T. G., Preda, A., Nguyen, D., Faziola, L., Turner, J., Bustillo, J., Belger, A., Lim, K. O., McEwen, S., Voyvodic, J., et al. (2014). Converting positive and negative symptom scores between panss and saps/sans. *Schizophrenia research*, 152(1):289–294.

[82] Van Erp, T. G., Walton, E., Hibar, D. P., Schmaal, L., Jiang, W., Glahn, D. C., Pearlson, G. D., Yao, N., Fukunaga, M., Hashimoto, R., et al. (2018). Cortical brain abnormalities in 4474 individuals with schizophrenia and 5098 control subjects via the enhancing neuro imaging genetics through meta analysis (enigma) consortium. *Biological Psychiatry*, 84(9):644–654.

[83] Vértes, P. E., Rittman, T., Whitaker, K. J., Romero-Garcia, R., Váša, F., Kitzbichler, M. G., Wagstyl, K., Fonagy, P., Dolan, R. J., Jones, P. B., et al. (2016). Gene transcription profiles associated with inter-modular hubs and connection distance in human functional magnetic resonance imaging networks. *Phil Trans R Soc B*, 371(1705):20150362.

[84] von Economo, C. F. and Koskinas, G. N. (1925). *Die cytoarchitektonik der hirnrinde des erwachsenen menschen*. J. Springer.

[85] von Economo, C. F., Koskinas, G. N., and Triarhou, L. C. (2008). Atlas of cytoarchitectonics of the adult human cerebral cortex.

[86] Wannan, C., Cropley, V., Chakravarty, M., Bousman, C., Bruggemann, J., Wickert, T., Shannon-Weickert, C., Everall, I., McGorry, P., Velakoulis, D., Wood, S., Bartholomeusz, C., Pantelis, C., and Zalesky, A. (2018). Connectivity shapes cortical thickness reductions in schizophrenia: 'regions that link together, thin together'. *under review*.

[87] Warren, J. D., Rohrer, J. D., Schott, J. M., Fox, N. C., Hardy, J., and Rossor, M. N. (2013). Molecular nexopathies: a new paradigm of neurodegenerative disease. *Trends Neurosci*, 36(10):561–569.

[88] Watanabe, Y., Someya, T., and Nawa, H. (2010). Cytokine hypothesis of schizophrenia pathogenesis: evidence from human studies and animal models. *Psychiat Clin Neurosci*, 64(3):217–230.

[89] Whitaker, K. J., Vértes, P. E., Romero-Garcia, R., Váša, F., Moutoussis, M., Prabhu, G., Weiskopf, N., Callaghan, M. F., Wagstyl, K., Rittman, T., et al. (2016). Adolescence is associated with genomically patterned consolidation of the hubs of the human brain connectome. *Proceedings of the National Academy of Sciences*, 113(32):9105–9110.

[90] White, T. P., Joseph, V., Francis, S. T., and Liddle, P. F. (2010). Aberrant salience network (bilateral insula and anterior cingulate cortex) connectivity during information processing in schizophrenia. *Schizophrenia Res*, 123(2-3):105–115.

[91] Woods, S. W. (2003). Chlorpromazine equivalent doses for the newer atypical antipsychotics. *J Clin Psychiat*.

[92] Yau, Y., Zeighami, Y., Baker, T., Larcher, K., Vainik, U., Dadar, M., Fonov, V., Hagmann, P., Griffa, A., Mišić, B., et al. (2018). Network connectivity determines cortical thinning in early parkinsonâĂŹs disease progression. *Nat Commun*, 9(1):12.

[93] Yeo, B. T., Krienen, F. M., Sepulcre, J., Sabuncu, M. R., Lashkari, D., Hollinshead, M., Roffman, J. L., Smoller, J. W., Zöllei, L., Polimeni, J. R., et al. (2011). The organization of the human cerebral cortex estimated by intrinsic functional connectivity. *Journal of Neurophysiology*, 106(3):1125–1165.

[94] Zalesky, A., Fornito, A., Seal, M. L., Cocchi, L., Westin, C.-F., Bullmore, E. T., Egan, G. F., and Pantelis, C. (2011). Disrupted axonal fiber connectivity in schizophrenia. *Biol Psychiat*, 69(1):80–89.

[95] Zeighami, Y., Ulla, M., Iturria-Medina, Y., Dadar, M., Zhang, Y., Larcher, K. M.-H., Fonov, V., Evans, A. C., Collins, D. L., and Dagher, A. (2015). Network structure of brain atrophy in de novo parkinson's disease. *Elife*, 4:e08440.

[96] Zheng, Y.-Q., Zhang, Y., Yau, Y. H., Zeighami, Y., Larcher, K., Misic, B., and Dagher, A. (2018). Connectome architecture, gene expression and functional coactivation shape the propagation of misfolded proteins in neurodegenerative disease. *bioRxiv*, page 449199.

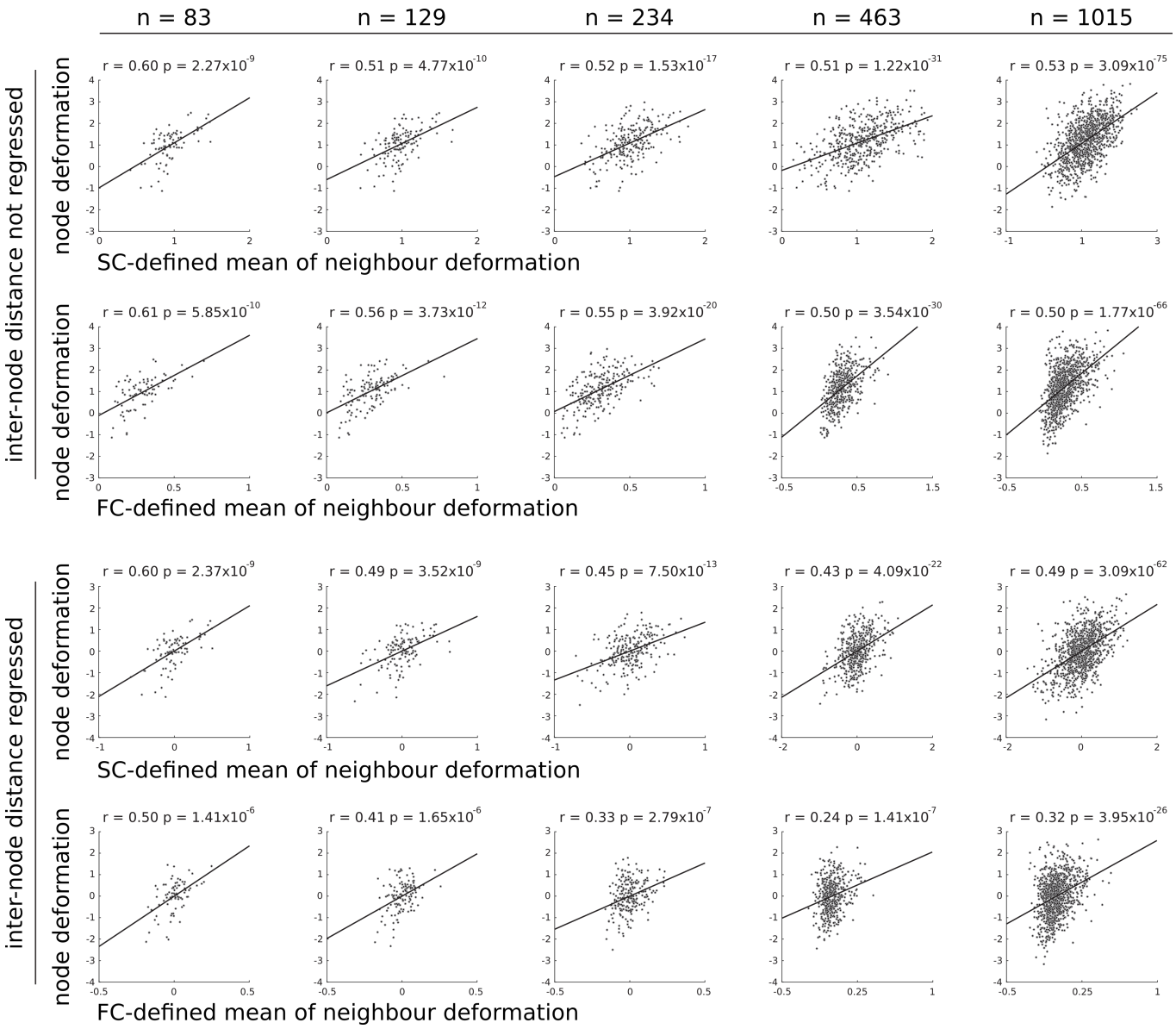

Figure S1. **Network-dependent deformation (contrasting schizophrenia patients and controls) |** Deformation is defined using a general linear model to identify regions where deformation is different between patients with schizophrenia and controls (controlling for age). The deformation of a node is correlated with the deformation of connected neighbours, defined by structural connectivity (SC) and functional connectivity (FC). Top and bottom: Results are shown with and without removing the effect of spatial proximity. Left to right: Correlations are shown for five progressively finer anatomical parcellations [13].

TABLE S1. The relationship between deformation of a node and its neighbours for schizophrenia patients was estimated using a multiple regression model, where deformation values of structurally- and functionally- defined neighbours were simultaneously included as predictors.

	n=83	**n=129**	**n=234**	**n=463**	**n=1015**
inter-node distance not regressed:					
adjusted-r	0.63	0.57	0.57	0.53	0.55
P-value	6.78×10^{-10}	6.68×10^{-12}	7.23×10^{-21}	7.36×10^{-35}	5.13×10^{-82}
inter-node distance regressed:					
adjusted-r	0.63	0.54	0.48	0.43	0.50
P-value	5.28×10^{-10}	1.70×10^{-10}	3.06×10^{-14}	4.49×10^{-22}	2.88×10^{-64}

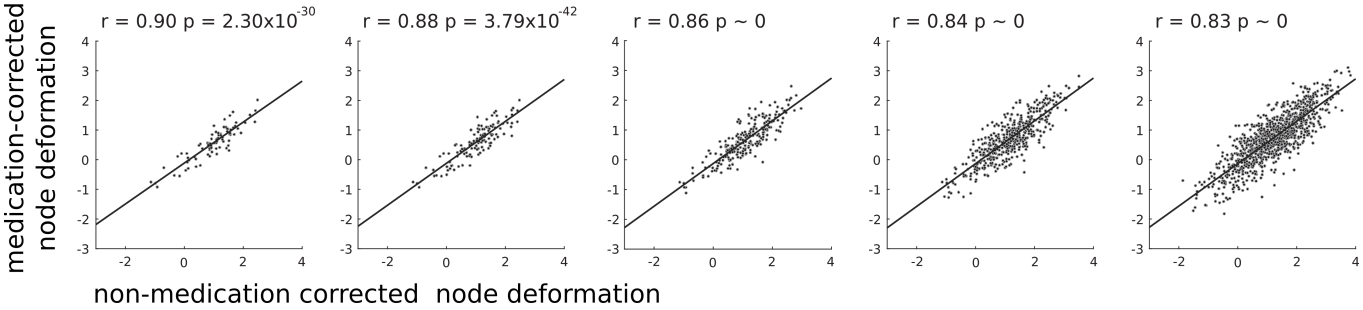

Figure S2. **Relationship between medication-corrected and non-medication corrected deformation maps |** Deformation is defined using a general linear model (controlling for age) to identify regions where deformation is different between patients with schizophrenia and controls. The analysis was repeated for a subset of patients for whom the chlorpromazine equivalent antipsychotic medication dose information was available. Both medication dose and age were included as covariates in the second analysis. The medication-corrected and non-medication corrected node deformation values are highly correlated. Left to right: Correlations are shown for five progressively finer anatomical parcellations [13].

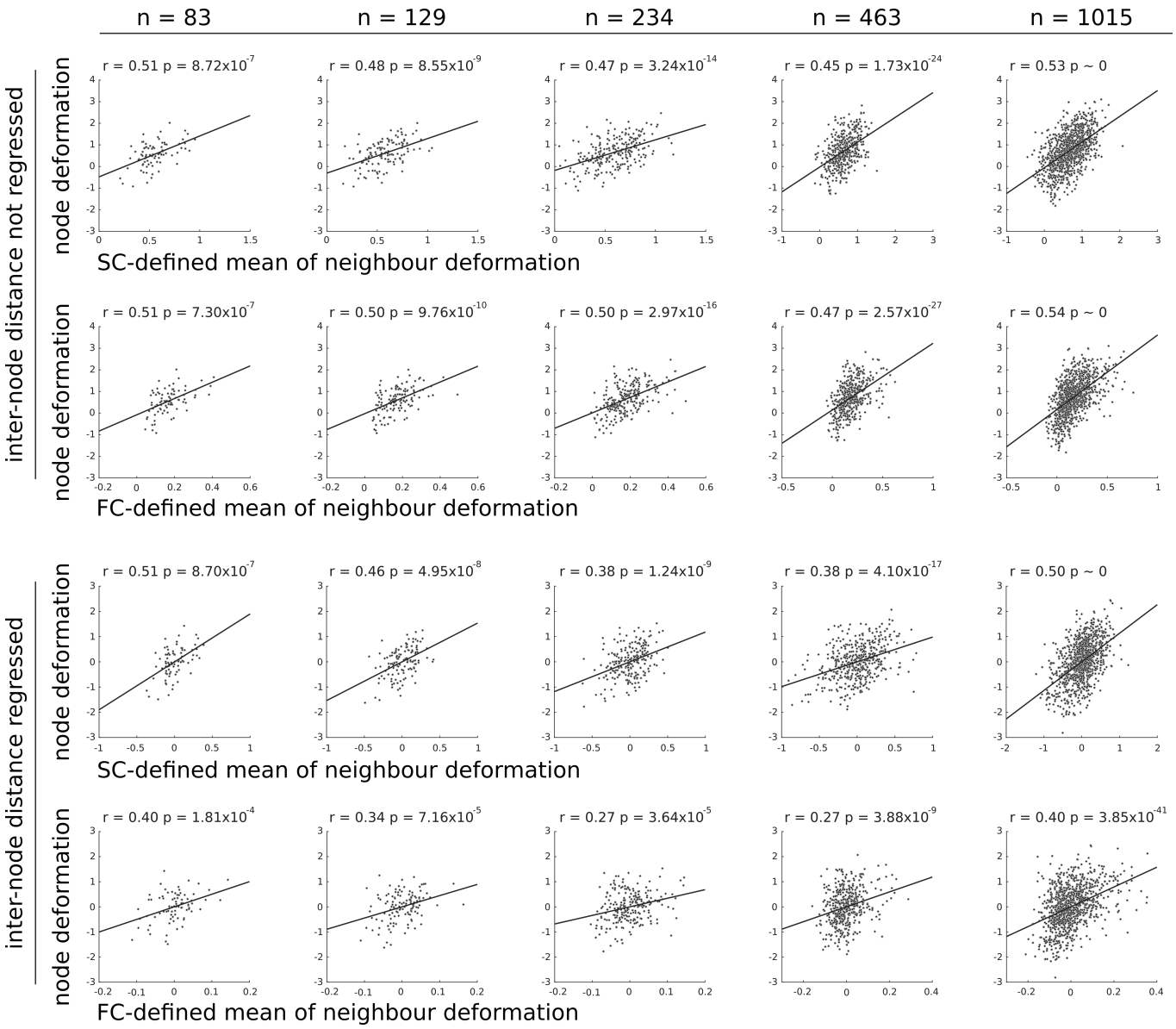

Figure S3. **Network-dependent deformation controlling for medication dose |** Medication-corrected deformation was defined for a subset of patients ($N = 87$) for whom the chlorpromazine equivalent antipsychotic medication dose information was available. A general linear model was used to identify regions where deformation is different between patients with schizophrenia and controls, controlling for medication dose and age. The deformation of a node is correlated with the deformation of connected neighbours, defined by structural connectivity (SC) and functional connectivity (FC). Top and bottom: Results are shown with and without removing the effect of spatial proximity. Left to right: Correlations are shown for five progressively finer anatomical parcellations [13].

TABLE S2. **GO terms associated with greater brain tissue volume deformation |** GOrilla was used to identify GO terms and biological processes associated with greater deformation in schizophrenia patients. Results were subdivided into clusters using REViGO and are shown for the third parcellation resolution (i.e., 234 nodes). Cluster labels are shown in bold and ranked according to P-values. If applicable, biological processes are also shown for each cluster (ranked by P-value).

Go term ID	Biological process	P-value	FDR q-value	Enrichment
GO:0051960	**Regulation of nervous system development**	**6.18E-10**	**3.64E-06**	**1.47**
GO:2000026	Regulation of multicellular organismal development	2.95E-10	3.48E-06	1.33
GO:0060284	Regulation of cell development	3.52E-09	1.38E-05	1.45
GO:0051962	Positive regulation of nervous system development	9.38E-09	1.58E-05	1.58
GO:0045664	Regulation of neuron differentiation	5.58E-08	4.38E-05	1.49
GO:0050767	Regulation of neurogenesis	6.18E-08	4.55E-05	1.44
GO:0010975	Regulation of neuron projection development	9.63E-08	6.67E-05	1.53
GO:0045666	Positive regulation of neuron differentiation	2.05E-07	1.21E-04	1.64
GO:0045595	Regulation of cell differentiation	1.46E-06	5.75E-04	1.30
GO:0051240	Positive regulation of multicellular organismal process	1.70E-06	6.45E-04	1.32
GO:0010720	Positive regulation of cell development	1.89E-06	6.96E-04	1.49
GO:0010976	Positive regulation of neuron projection development	2.02E-06	7.22E-04	1.70
GO:0050769	Positive regulation of neurogenesis	3.32E-06	1.09E-03	1.51
GO:0010769	Regulation of cell morphogenesis involved in differentiation	7.15E-06	2.05E-03	1.81
GO:0050770	Regulation of axonogenesis	7.39E-06	2.02E-03	2.00
GO:0022603	Regulation of anatomical structure morphogenesis	9.67E-06	2.42E-03	1.36
GO:0022604	Regulation of cell morphogenesis	1.46E-05	3.36E-03	1.47
GO:0051094	Positive regulation of developmental process	2.10E-05	4.57E-03	1.31
GO:0120039	Plasma membrane bounded cell projection morphogenesis	5.12E-05	9.73E-03	1.63
GO:0048812	Neuron projection morphogenesis	5.38E-05	1.01E-02	1.63
GO:0048858	Cell projection morphogenesis	7.44E-05	1.27E-02	1.61
GO:0032879	**Regulation of localization**	**6.43E-09**	**1.89E-05**	**1.36**
GO:0051239	**Regulation of multicellular organismal process**	**6.62E-09**	**1.56E-05**	**1.25**
GO:0031344	**Regulation of cell projection organization**	**9.32E-09**	**1.83E-05**	**1.51**
GO:0120035	Regulation of plasma membrane bounded cell projection organization	1.48E-08	1.93E-05	1.50
GO:0031346	Positive regulation of cell projection organization	2.21E-07	1.24E-04	1.62
GO:0051130	Positive regulation of cellular component organization	4.65E-05	8.98E-03	1.26
GO:0050793	**Regulation of developmental process**	**1.09E-08**	**1.60E-05**	**1.27**
GO:0048731	**System development**	**1.59E-08**	**1.87E-05**	**1.71**
GO:0048856	Anatomical structure development	1.67E-05	3.70E-03	1.21
GO:0007399	Nervous system development	2.16E-05	4.54E-03	1.71
GO:0099536	**Synaptic signaling**	**3.09E-08**	**3.31E-05**	**1.88**
GO:0099537	Trans-synaptic signaling	3.09E-08	3.03E-05	1.88
GO:0099177	Regulation of trans-synaptic signaling	4.98E-08	4.52E-05	1.56
GO:0050804	Modulation of synaptic transmission	4.98E-08	4.19E-05	1.56
GO:0007268	Chemical synaptic transmission	5.58E-07	2.63E-04	1.85
GO:0098916	Anterograde trans-synaptic signaling	5.58E-07	2.74E-04	1.85
GO:0023052	**Signaling**	**1.28E-07**	**8.41E-05**	**1.68**
GO:0007267	**Cell-cell signaling**	**1.94E-07**	**1.20E-04**	**1.70**
GO:1903530	**Regulation of secretion by cell**	**3.04E-07**	**1.63E-04**	**1.51**
GO:0051049	Regulation of transport	5.53E-07	2.83E-04	1.31
GO:0051046	Regulation of secretion	2.51E-06	8.70E-04	1.48
GO:1903305	Regulation of regulated secretory pathway	8.19E-06	2.14E-03	1.87
GO:0017158	Regulation of calcium ion-dependent exocytosis	1.50E-05	3.39E-03	1.91
GO:0017157	Regulation of exocytosis	4.03E-05	8.04E-03	1.72
GO:0000165	**MAPK cascade**	**8.18E-07**	**3.70E-04**	**1.79**
GO:0023014	Signal transduction by protein phosphorylation	1.43E-06	5.79E-04	1.73
GO:0016310	Phosphorylation	8.05E-06	2.16E-03	1.38
GO:0006468	Protein phosphorylation	6.34E-05	1.11E-02	1.36
GO:0032502	**Developmental process**	**8.29E-07**	**3.62E-04**	**1.16**
GO:0007165	**Signal transduction**	**1.00E-06**	**4.22E-04**	**1.18**
GO:0023051	**Regulation of signaling**	**3.27E-06**	**1.10E-03**	**1.32**
GO:0035556	**Intracellular signal transduction**	**4.16E-06**	**1.32E-03**	**1.30**
GO:0007610	**Behaviour**	**4.42E-06**	**1.37E-03**	**1.59**
GO:0010646	**Regulation of cell communication**	**5.14E-06**	**1.55E-03**	**1.31**

GO terms associated with greater deformation (Cont.)				
Go term ID	**Biological process**	***P*-value**	**FDR *q*-value**	**Enrichment**
GO:0098655	**Cation transmembrane transport**	**6.79E-06**	**2.00E-03**	**1.71**
GO:0030001	Metal ion transport	7.16E-06	2.01E-03	1.61
GO:0098662	Inorganic cation transmembrane transport	8.88E-06	2.27E-03	1.72
GO:0006812	Cation transport	1.03E-05	2.53E-03	1.73
GO:0043269	Regulation of ion transport	1.27E-05	2.98E-03	1.79
GO:0098660	Inorganic ion transmembrane transport	2.15E-05	4.60E-03	1.64
GO:0034762	Regulation of transmembrane transport	6.88E-05	1.19E-02	1.51
GO:0034765	Regulation of ion transmembrane transport	8.55E-05	1.40E-02	1.42
GO:0098693	Regulation of synaptic vesicle cycle	8.59E-05	1.39E-02	1.75
GO:0007154	**Cell communication**	**1.07E-05**	**2.58E-03**	**1.49**
GO:0044057	**Regulation of system process**	**2.19E-05**	**4.52E-03**	**1.52**
GO:0051056	**Regulation of small GTPase mediated signal transduction**	**2.33E-05**	**4.73E-03**	**2.19**
GO:0006811	**Ion transport**	**4.19E-05**	**8.23E-03**	**1.49**
GO:0050794	**Regulation of cellular process**	**5.43E-05**	**9.99E-03**	**1.06**
GO:0043087	**Regulation of GTPase activity**	**5.47E-05**	**9.91E-03**	**1.87**
GO:0090257	**Regulation of muscle system process**	**5.73E-05**	**1.02E-02**	**1.85**
GO:0099560	**Synaptic membrane adhesion**	**7.91E-05**	**1.33E-02**	**2.54**
GO:0030030	**Cell projection organization**	**8.35E-05**	**1.39E-02**	**1.32**

TABLE S3. **GO terms associated with lower brain tissue volume deformation |** GOrilla was used to identify GO terms and biological processes associated with lower deformation in schizophrenia patients. Results were subdivided into clusters using REViGO and are shown for the third parcellation resolution (i.e., 234 nodes). Cluster labels are shown in bold and ranked according to P-values. If applicable, biological processes are also shown for each cluster (ranked by P-value).

Go term ID	Biological process	P-value	FDR q-value	Enrichment
GO:0006955	**Immune response**	**4.62E-16**	**5.90E-12**	**3.61**
GO:0002684	Positive regulation of immune system process	1.16E-11	3.70E-08	3.08
GO:0002682	Regulation of immune system process	3.28E-10	8.39E-07	2.42
GO:0002253	Activation of immune response	1.00E-09	1.65E-06	3.88
GO:0050776	Regulation of immune response	2.58E-09	3.29E-06	2.84
GO:0050778	Positive regulation of immune response	8.93E-09	8.15E-06	3.25
GO:0045321	Leukocyte activation	2.66E-08	1.70E-05	1.49
GO:0002366	Leukocyte activation involved in immune response	1.31E-07	6.19E-05	1.56
GO:0002263	Cell activation involved in immune response	2.09E-07	8.91E-05	1.55
GO:0002252	Immune effector process	7.16E-07	2.41E-04	2.53
GO:0002696	Positive regulation of leukocyte activation	8.76E-07	2.73E-04	2.87
GO:0002275	Myeloid cell activation involved in immune response	1.39E-06	3.95E-04	1.55
GO:0050867	Positive regulation of cell activation	2.07E-06	5.50E-04	2.77
GO:0002757	Immune response-activating signal transduction	2.73E-06	6.85E-04	3.42
GO:0002274	Myeloid leukocyte activation	3.95E-06	9.52E-04	1.50
GO:0002283	Neutrophil activation involved in immune response	4.03E-06	9.53E-04	1.54
GO:0042119	Neutrophil activation	5.45E-06	1.22E-03	1.53
GO:0043299	Leukocyte degranulation	6.96E-06	1.43E-03	1.52
GO:0002764	Immune response-regulating signaling pathway	1.01E-05	1.95E-03	3.19
GO:0043312	Neutrophil degranulation	1.03E-05	1.97E-03	1.52
GO:0036230	Granulocyte activation	1.08E-05	2.00E-03	1.51
GO:0050671	Positive regulation of lymphocyte proliferation	1.09E-05	1.98E-03	10.95
GO:0042102	Positive regulation of T cell proliferation	1.21E-05	2.16E-03	13.42
GO:0032946	Positive regulation of mononuclear cell proliferation	1.23E-05	2.14E-03	10.78
GO:0002697	Regulation of immune effector process	1.29E-05	2.23E-03	3.63
GO:0070665	Positive regulation of leukocyte proliferation	1.38E-05	2.35E-03	10.62
GO:0002694	Regulation of leukocyte activation	1.70E-05	2.79E-03	2.19
GO:0050670	Regulation of lymphocyte proliferation	3.58E-05	5.08E-03	7.92
GO:0002218	Activation of innate immune response	3.79E-05	5.32E-03	4.25
GO:0032944	Regulation of mononuclear cell proliferation	3.87E-05	5.37E-03	7.84
GO:0002922	Positive regulation of humoral immune response	4.20E-05	5.71E-03	348.89
GO:0070663	Regulation of leukocyte proliferation	4.37E-05	5.81E-03	7.76
GO:0050900	Leukocyte migration	4.38E-05	5.70E-03	1.86
GO:0050865	Regulation of cell activation	4.53E-05	5.84E-03	2.08
GO:0002687	Positive regulation of leukocyte migration	7.10E-05	8.40E-03	13.76
GO:0006952	**Defense response**	**3.15E-12**	**2.01E-08**	**3.28**
GO:0002376	**Immune system response**	**8.15E-12**	**3.47E-08**	**2.22**
GO:0006614	**SRP-dependent cotranslational protein targeting to membrane**	**1.00E-09**	**1.86E-06**	**2.09**
GO:0006613	Cotranslational protein targeting to membrane	2.80E-09	3.25E-06	2.04
GO:0045047	Protein targeting to ER	7.00E-09	7.42E-06	2.00
GO:0072599	Establishment of protein localization to endoplasmic reticulum	1.53E-08	1.08E-05	1.97
GO:0070972	Protein localization to endoplasmic reticulum	1.28E-07	6.27E-05	1.90
GO:0006612	Protein targeting to membrane	7.88E-07	2.52E-04	1.76
GO:0006605	Protein targeting	6.38E-05	7.62E-03	1.43
GO:0098581	**Detection of external biotic stimulus**	**1.25E-08**	**9.99E-06**	**25.49**
GO:0061844	Antimicrobial humoral immune response (by antimicrobial peptide)	1.29E-09	1.83E-06	3.88
GO:0042742	Defense response to bacterium	8.31E-09	8.16E-06	2.80
GO:0009617	Response to bacterium	1.25E-08	9.43E-06	2.40
GO:0032490	Detection of molecule of bacterial origin	1.25E-08	1.07E-05	25.49
GO:0051707	Response to other organism	2.30E-08	1.54E-05	1.79
GO:0019730	Antimicrobial humoral response	1.84E-07	8.11E-05	3.31
GO:0043207	Response to external biotic stimulus	5.57E-07	1.98E-04	1.42
GO:0050830	Defense response to Gram-positive bacterium	1.14E-06	3.48E-04	3.96
GO:0098542	Defense response to other organism	1.15E-06	3.41E-04	2.56
GO:0032101	Regulation of response to external stimulus	1.92E-06	5.23E-04	2.85
GO:0019731	Antibacterial humoral response	5.10E-05	6.45E-03	4.66
GO:0050829	Defense response to Gram-negative bacterium	8.06E-05	9.20E-03	7.32
GO:0002920	Regulation of humoral immune response	9.80E-05	1.07E-02	30.66

GO terms associated with lower deformation (Cont.)				
Go term ID	**Biological process**	***P*-value**	**FDR *q*-value**	**Enrichment**
GO:0006954	**Inflammatory response**	**4.16E-08**	**2.53E-05**	**3.62**
GO:0045087	Innate immune response	3.63E-10	7.72E-07	3.72
GO:0031347	Regulation of defense response	1.95E-05	3.16E-03	2.50
GO:0006959	**Humoral immune response**	**7.15E-08**	**4.15E-05**	**5.83**
GO:0042116	**Macrophage activation**	**9.73E-08**	**5.41E-05**	**10.13**
GO:0009595	**Detection of biotic stimulus**	**1.04E-07**	**5.51E-05**	**21.85**
GO:0002227	**Innate immune response in mucosa**	**1.53E-07**	**6.99E-05**	**7.00**
GO:0002385	Mucosal immune response	7.83E-06	1.56E-03	5.72
GO:0042035	**Regulation of cytokine biosynthetic process**	**2.31E-07**	**9.24E-05**	**5.01**
GO:0042108	Positive regulation of cytokine biosynthetic process	3.74E-06	9.18E-04	6.69
GO:0001819	Positive regulation of cytokine production	8.38E-06	1.65E-03	5.66
GO:0032722	Positive regulation of chemokine production	1.38E-05	2.32E-03	9.41
GO:0032677	Regulation of interleukin-8 production	5.94E-05	7.23E-03	6.75
GO:0032642	Regulation of chemokine production	8.26E-05	9.34E-03	6.62
GO:0001775	**Cell activation**	**2.89E-07**	**1.12E-04**	**1.43**
GO:0045785	**Positive regulation of cell adhesion**	**4.50E-07**	**1.64E-04**	**6.64**
GO:1903039	Positive regulation of leukocyte cell-cell adhesion	1.09E-07	5.56E-05	10.78
GO:0022409	Positive regulation of cell-cell adhesion	3.43E-07	1.29E-04	9.68
GO:1903037	Regulation of leukocyte cell-cell adhesion	4.04E-06	9.39E-04	7.65
GO:0050870	Positive regulation of T cell activation	1.07E-05	2.00E-03	9.13
GO:0022407	Regulation of cell-cell adhesion	2.00E-05	3.20E-03	5.75
GO:0030155	Regulation of cell adhesion	2.49E-05	3.78E-03	4.13
GO:1904996	Positive regulation of leukocyte adhesion to vascular endothelial cell	5.55E-05	6.96E-03	133.05
GO:1903238	Positive regulation of leukocyte tethering or rolling	5.55E-05	6.89E-03	133.05
GO:0000956	**Nuclear-transcribed mRNA catabolic process**	**7.02E-07**	**2.42E-04**	**2.6**
GO:0000184	Nuclear-transcribed mRNA catabolic process, nonsense-mediated decay	2.24E-07	9.24E-05	1.99
GO:0006402	mRNA catabolic process	6.33E-06	1.35E-03	2.40
GO:0006401	RNA catabolic process	1.42E-05	2.36E-03	2.24
GO:0046700	Heterocycle catabolic process	3.37E-05	4.84E-03	1.90
GO:0034655	Nucleobase-containing compound catabolic process	9.03E-05	9.95E-03	1.88
GO:0035589	**G protein-coupled purinergic nucleotide receptor signaling pathway**	**7.72E-07**	**2.53E-04**	**66.95**
GO:0035590	Purinergic nucleotide receptor signaling pathway	6.77E-06	1.42E-03	46.87
GO:0035588	G protein-coupled purinergic receptor signaling pathway	1.17E-05	2.11E-03	42.61
GO:0002761	**Regulation of myeloid leukocyte differentiation**	**1.20E-06**	**3.48E-04**	**7.23**
GO:0045670	Regulation of osteoclast differentiation	2.73E-05	4.00E-03	8.83
GO:0055094	**Response to lipoprotein particle**	**1.41E-06**	**3.91E-04**	**9.31**
GO:0009607	**Response to biotic stimulus**	**2.14E-06**	**5.58E-04**	**1.39**
GO:0007166	**Cell surface receptor signaling pathway**	**2.33E-06**	**5.95E-04**	**1.33**
GO:0071402	**Cellular response to lipoprotein particle stimulus**	**4.24E-06**	**9.68E-04**	**8.54**
GO:0034447	**Very-low-density lipoprotein particle clearance**	**5.65E-06**	**1.25E-03**	**785.00**
GO:0034379	Very-low-density lipoprotein particle assembly	5.65E-06	1.22E-03	785.00
GO:0006413	**Translational initiation**	**7.55E-06**	**1.53E-03**	**2.61**
GO:0006412	Translation	4.37E-05	5.76E-03	2.08
GO:0043043	Peptide biosynthetic process	4.84E-05	6.18E-03	2.04
GO:0002181	Cytoplasmic translation	8.87E-05	9.94E-03	4.09
GO:0031640	**Killing of cells of other organism**	**2.33E-05**	**3.63E-03**	**10.01**
GO:0044364	Disruption of cells of other organism	2.33E-05	3.67E-03	10.01
GO:1901361	**Organic cyclic compound catabolic process**	**2.36E-05**	**3.64E-03**	**1.87**
GO:0048584	**Positive regulation of response to stimulus**	**2.59E-05**	**3.85E-03**	**1.71**
GO:0002251	**Organ or tissue specific immune response**	**3.11E-05**	**4.52E-03**	**5.25**
GO:0006334	**Nucleosome assembly**	**3.96E-05**	**5.44E-03**	**2.74**
GO:0034728	Nucleosome organization	2.50E-05	3.76E-03	2.39
GO:0035587	**Purinergic receptor signaling pathway**	**4.27E-05**	**5.74E-03**	**33.48**
GO:0019221	**Cytokine-mediated signaling pathway**	**5.76E-05**	**7.08E-03**	**1.49**
GO:1901698	**Response to nitrogen compound**	**6.25E-05**	**7.54E-03**	**2.20**
GO:0006887	**Exocytosis**	**7.27E-05**	**8.52E-03**	**1.40**
GO:0006911	**Phagocytosis, engulfment**	**7.29E-05**	**8.47E-03**	**11.54**
GO:0002886	**Regulation of myeloid leukocyte mediated immunity**	**7.82E-05**	**9.00E-03**	**2.78**
GO:0071824	**Protein-DNA complex subunit organization**	**8.95E-05**	**9.94E-03**	**2.25**